POLITECNICO DI TORINO

Master's Degree Course in

MATERIALS ENGINEERING FOR INDUSTRY 4.0

College of Chemical and Materials Engineering

Master's Thesis

UV and Thermal curing of biobased coatings with covalent adaptable network properties: Joule Heating-Induced Reprocessability

Politecnico di Torino

Supervisor:
Marco Sangermano

Candidate:
Greppi Serena

July 2026

Index:

1. Introduction

Modern society is deeply dependent on polymeric materials, which have become indispensable in everyday life due to their versatility, durability, and cost-effectiveness. Polymers are extensively employed in a wide range of applications, including structural, medical, scientific, and technological fields, significantly contributing to social and industrial development. However, the widespread use of plastics has also generated severe environmental concerns. (1)

Over the last decades, global production of polymer resins and plastics has increased suddently (Figure 1), reaching the highest levels. Projections indicate that, by 2050, plastic production could account for approximately 20% of the world's fossil fuel consumption. (2)(3)

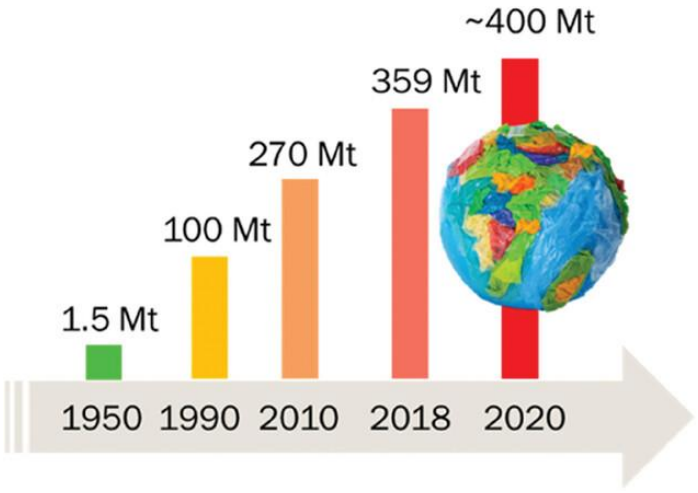

Figure 1 - Worldwide annual production of plastics from 1950 to 2020.

Simultaneously with the continuous growth of the plastics industry, the generation of plastic waste has also increased dramatically. If not properly managed and disposed of, plastic waste can severely affect both terrestrial and marine ecosystems. This scenario is further aggravated by unsustainable patterns of resource consumption, as humanity currently exploits natural resources at a rate exceeding the Earth's regenerative capacity.

The environmental issues associated with the fossil-based origin of conventional polymers, together with the accumulation of persistent plastic waste, urgently call for the development of more sustainable materials and circular approaches. In this context, the exploitation of renewable and biobased resources as alternative polymer precursors has emerged as a promising strategy.

Among the different classes of sustainable materials, biobased thermosetting polymers have attracted increasing attention as promising alternatives to conventional petroleum-derived thermosets, such as bisphenol A-based epoxy resins (6). The term “biobased” refers to a product synthesized from renewable resources and does not imply biodegradability (7).

The following sections briefly describe the synthesis routes adopted for the preparation of the two polymer matrices investigated in this work: diglycidyl ether of vanillyl alcohol (DGEVA) and epoxidized castor oil (ECO). Particular attention is given to the renewable origin of the precursors and to the chemical processes involved in obtaining these bio-based epoxy systems.

As a concrete example of a biobased production route, the diglycidyl ether of vanillyl alcohol (DGEVA), investigated in this work, can be synthesized starting from lignin-derived compounds. Lignin is one of the most abundant aromatic biopolymers in the biosphere and represents a highly promising renewable feedstock for the production of aromatic chemicals. The pulp and paper industry is currently the major source of lignin, with the Kraft process (4) accounting for approximately 80% of the global production of chemical pulp. Black liquor, the main by-product of the Kraft process, typically contains 30–34 wt.% lignin. Through appropriate valorization strategies, lignin can be converted into valuable platform molecules, such as vanillin, which can subsequently be used for the synthesis of biobased epoxy monomers. Figure 2 illustrates an overview of the proposed process flow for the production of vanillin from lignin. The scheme represents the entire conversion pathway, highlighting how each by-product generated during the different processing stages can be further valorized to obtain additional high-value compounds. This approach is consistent with the concept of integrated biomass valorization, in which no stream is regarded as waste; instead, each fraction can be recovered and converted into a useful product. As a result, the overall sustainability, resource efficiency, and economic viability of the process can be significantly enhanced (4).

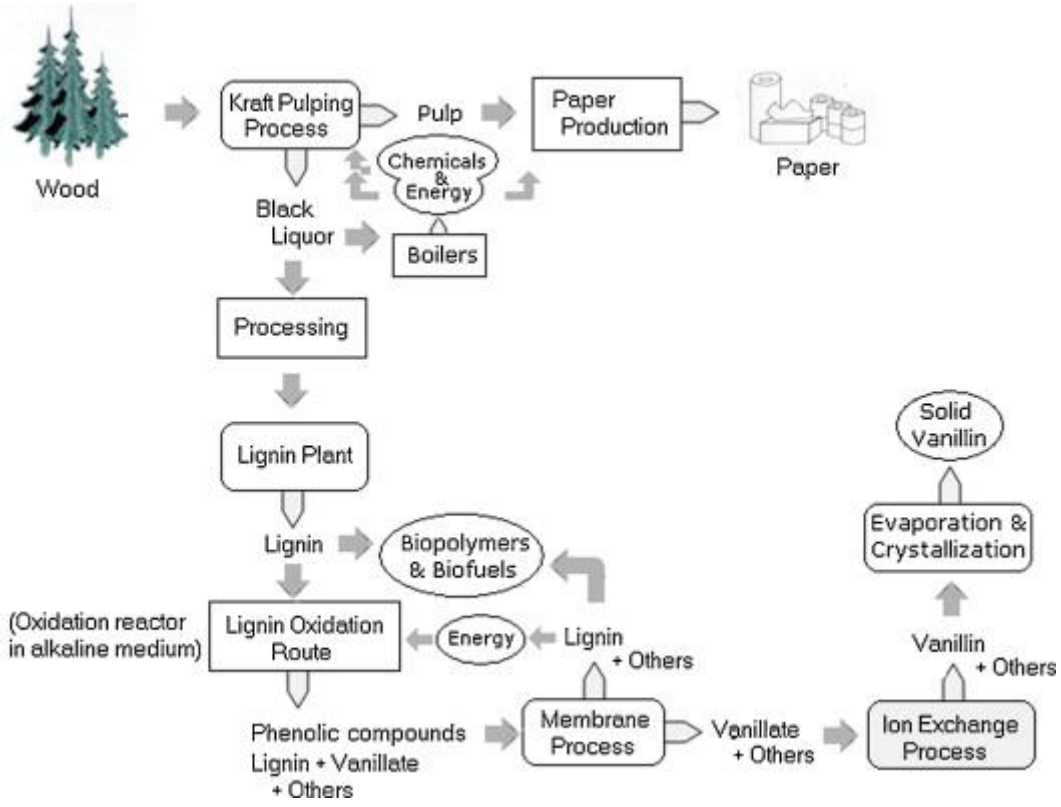

Figure 2 - Valorization of Kraft lignin through a biorefinery approach: the proposed integrated process for the production of vanillin and biopolymers (4)

Another possible approach to address these challenges is the valorization of the large quantities of agricultural and food waste generated annually worldwide, a trend that is expected to intensify with the continuous growth of the global population. An example of oils that can be used for the production of bio-based products is shown in Figure 3.

Figure 3 - Common botanic oils used in cationic UV curing systems (5)

The conversion of these biomass residues into high-value products represents a key opportunity for promoting sustainability while reducing environmental impact (6). Nevertheless, the heterogeneous nature of biomass feedstocks, characterized by significant variations in their physicochemical properties, makes their processing and conversion particularly challenging. Despite this complexity, biomass-derived polymers are naturally abundant and can be selectively extracted, chemically modified, or depolymerized to obtain a wide range of valuable chemical intermediates and polymeric building blocks.

As a matter of fact, the increasing market interest in biobased materials and research activities are mainly focused on increasing the performances and durability instead of the biodegradability.

In particular, the combination of renewable feedstocks with dynamic covalent chemistry, which will be discussed in detail in Section 1.3, has enabled the development of biobased epoxy covalent adaptable networks (CANs). These materials represent a novel class of polymer networks that combine the outstanding thermal and mechanical properties of traditional thermosets with additional features such as recyclability, reprocessability, and healing capability (7).

Due to the presence of dynamic covalent bonds, CANs behave as permanently crosslinked materials under service conditions, while being able to undergo network rearrangements above a characteristic temperature known as the topology freezing transition temperature (*T*v). This unique behaviour makes biobased epoxy CANs highly attractive candidates for facilitating the transition toward a more sustainable and circular polymer economy.

As mentioned above, the epoxy resins investigated in this thesis are both derived from renewable resources. The first system is based on epoxidized castor oil, while the second consists of diglycidyl ether of vanillyl alcohol. Both materials were specifically designed to exhibit covalent adaptable network (CAN) behaviour through the incorporation of suitable dynamic functionalities. In the ECO-based formulation, dibutyl phosphate was introduced to promote transesterification reactions, whereas in the DGEVA system 4-aminophenyl disulfide (4-AFD) was employed to enable disulfide exchange reactions.

In the present work, these characteristics were exploited for the development of functional coatings with intrinsic healing properties, in accordance with the principles of sustainability and circular economy.

The two resin systems also differ in their curing mechanisms: the ECO formulation undergoes photopolymerization, whereas the DGEVA-based system is thermally cured. Therefore, the following chapters provide a theoretical overview of the main differences between these two classes of materials, the mechanisms governing the specific CAN chemistries involved, and the role and applications of electrically conductive polymers obtained through the incorporation of recycled carbon fibers.

1.1 UV curing

As previously mentioned, the ECO-based system investigated in this work is cured through a UV-induced polymerization process. Therefore, this section first introduces the general principles of UV curing before discussing the specific cationic mechanism involved in the ECO formulation.

The use of UV-curable formulations has increased considerably over the last decades owing to several advantages over conventional thermal curing processes. Among the most significant benefits are the extremely rapid curing rates, typically ranging from a few seconds to a few minutes, and the possibility of processing materials at room temperature, which substantially reduces energy consumption. Furthermore, UV curing improves both space and energy efficiency, since the curing equipment is generally much more compact than conventional thermal ovens. Additional advantages include the possibility of obtaining high-resolution patterns and the widespread use of solvent-free formulations, making this technology particularly attractive for advanced engineering applications. (8)

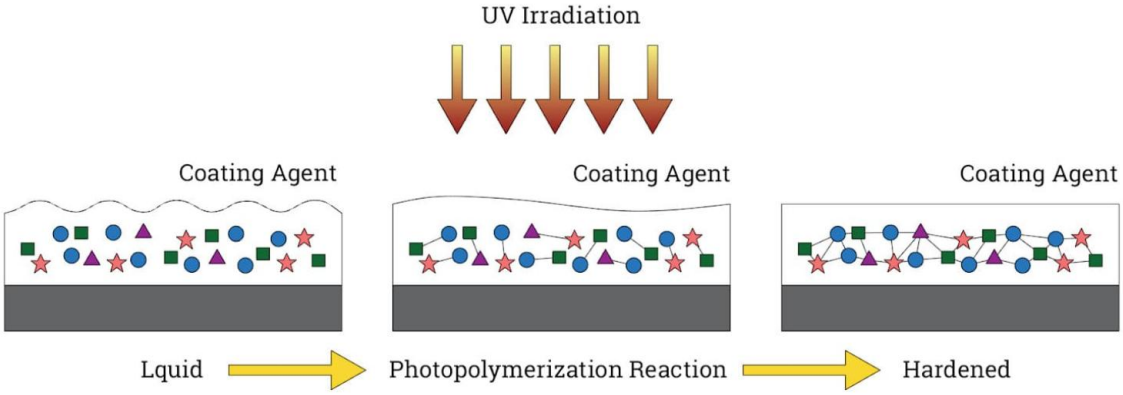

Figure 4 – Coating UV curing technique (9)

The curing process is based on photopolymerization, also referred to as photocuring, which consists of the rapid conversion of liquid formulations into crosslinked solid materials upon exposure to ultraviolet or visible radiation. In these systems, light is absorbed by a photosensitive compound, generating reactive species that initiate polymer network formation through chain reactions.

Photopolymerization exploits the energy carried by photons emitted in the low-wavelength region of the electromagnetic spectrum. The ultraviolet region, commonly employed in

photocuring applications, is generally divided into UV-A, UV-B, and UV-C ranges. The energy associated with a photon is given by:

$$E = h\nu = \frac{hc}{\lambda}$$

where ν is the frequency and λ is the wavelength. Since photon energy is inversely proportional to wavelength, shorter wavelengths correspond to higher energies. During the curing process, radiation acts solely as the initiating stimulus by generating reactive species and does not directly participate in the propagation or termination steps of the polymerization reaction, as schematically illustrated in Figure 5.

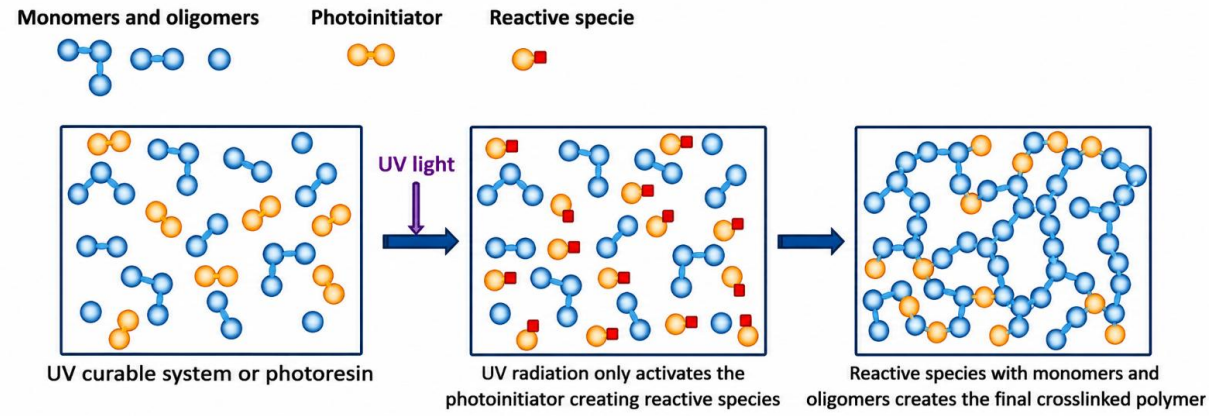

Figure 5 -Schematic representation of the photopolymerization process.

Despite its numerous advantages, UV curing also presents some limitations. Compared with thermal curing the complete curing through opaque or highly filled materials can be difficult because the intensity of the incident radiation decreases with the square of the distance from the light source, thereby reducing curing efficiency in regions not directly exposed to UV radiation. (10)

According to the nature of the reactive species generated during irradiation, UV-curable systems can be broadly classified into two categories: free-radical photopolymerization and ionic photopolymerization. The ECO-based formulation investigated in this work undergoes cationic photopolymerization, which offers several advantages over free-radical processes, (5,11) including:

- it does not require an inert atmosphere during the curing process, as it is not affected by oxygen inhibition.
- The process can continue even after the light source is removed. This phenomenon, known as a "dark reaction," can lead to further monomer conversion either at room temperature or through thermal post-treatment.

- Cationic photocurable monomers are generally characterized by low toxicity and low irritancy.
- The resulting materials exhibit reduced volumetric shrinkage upon curing and higher thermal resistance.

Epoxidized castor oil (ECO) was selected as the biobased monomer for this study because of its unique molecular structure (Figure 6). Unlike conventional epoxidized vegetable oils (EVOs), ECO contains hydroxyl groups along its fatty acid chains. The presence of these hydroxyl functionalities promotes chain-transfer reactions during cationic photopolymerization, resulting in higher polymerization rates and monomer conversion despite its lower epoxy functionality compared with other EVOs.

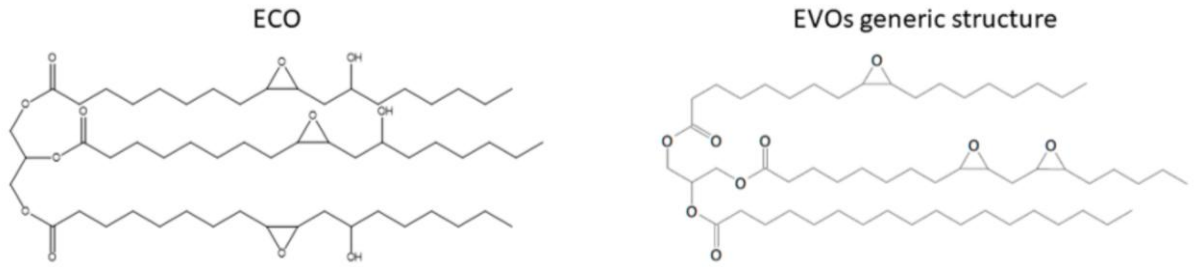

Figure 6 - ECO structure and generic EVOs structure

The nucleophilic attack of hydroxyl groups at the chain end of the growing ionic species leads to the formation of a protonated ether. Chain termination, occurring through proton transfer to a new epoxy monomer, can initiate the growth of a new polymer chain.

The kinetics of photopolymerization have also been investigated, including the effect of photosensitizers. In particular, the addition of the photosensitizer 2-isopropylthioxanthone (ITX) was shown to enhance the polymerization kinetics of ECO, which is why it was included in the formulation described in detail later in this work.

Previous studies have demonstrated the suitability of ECO for cationic UV curing. For instance, in 2019, the epoxidation of castor oil and its subsequent cationic photopolymerization using triphenylsulfonium hexafluoroantimonate as photoinitiator were investigated. The resulting polymer networks exhibited high conversion values (up to 85%) and good flexibility, highlighting the potential of ECO as a sustainable precursor for UV-curable materials. (12).

1.2 Thermal curing

Thermal curing is a widely employed technique for the processing of thermosetting polymers and composites. In this approach, heat is applied under controlled conditions to initiate the polymerization and crosslinking reactions of the resin matrix, which ultimately determine the network architecture and the resulting material properties. The curing process plays a crucial role in achieving the desired mechanical, thermal, and chemical performance of the final composite by ensuring a high degree of resin conversion and the formation of a stable three-dimensional crosslinked structure.

Typically, thermal curing is carried out through a programmed heat treatment using equipment such as convection ovens, hot presses, or autoclaves, where temperature and curing time are carefully controlled. During the process, thermal energy activates the reaction between the resin and the curing agent, progressively increasing the molecular weight of the system until gelation and subsequent vitrification occur. The final crosslink density achieved during curing strongly influences key properties such as stiffness, glass transition temperature (Tg), thermal stability, chemical resistance, and dimensional stability of the cured material. (13)

In the DGEVA system investigated in this work, thermal curing occurs through the reaction between the bio-based epoxy resin derived from vanillin and the aromatic diamine curing agent 4-AFD. Upon heating, the amine groups react with the epoxy rings through a nucleophilic ring-opening mechanism, generating hydroxyl groups and progressively building a densely crosslinked network. As a result, the initially liquid formulation is converted into a rigid thermoset exhibiting high mechanical strength, excellent dimensional stability, and enhanced thermal resistance.

1.3 CANs

Before discussing Covalent Adaptable Networks (CANs), it is useful to briefly introduce the conventional classification of polymeric materials, which are generally divided into two main categories: thermoplastics and thermosets. These two classes differ significantly in terms of molecular architecture, processing methods, and end-of-life management.

Thermoplastics consist of high-molecular-weight macromolecular chains that are not covalently interconnected but are instead held together through physical entanglements, resulting in topological constraints that limit molecular motion. When heated above a characteristic transition temperature, the polymer chains acquire sufficient mobility to diffuse through a mechanism known as reptation, leading to a progressive increase in material fluidity. Upon cooling, the polymer solidifies and retains the shape imposed during processing.

One of the main advantages of thermoplastics is their ability to undergo multiple heating and cooling cycles without undergoing significant chemical degradation, thereby enabling reprocessing and recycling. Their solidification behaviour depends strongly on their degree

of crystallinity and on the cooling conditions. In particular, semicrystalline thermoplastics exhibit a well-defined melting temperature (Tm), whereas amorphous thermoplastics undergo a gradual transition from a glassy to a rubbery state at the glass transition temperature (Tg) before reaching a viscous molten state. (14)

Figure 7 -Schematic representation of a thermoplastic polymer.

The ability to flow in the molten state allows their processing through industrial techniques such as extrusion and injection molding, while also facilitating recycling. However, thermoplastic polymers generally exhibit relatively low mechanical strength, are susceptible to degradation caused by heat, solvents, and environmental exposure, and experience a reduction in mechanical properties with increasing temperature.

Thermosets are cross-linked polymers characterized by a three-dimensional network formed through an irreversible polymerization process known as curing. This process typically occurs within a mold to achieve the final shape, as once completed, thermosets cannot be reshaped or reprocessed. At the molecular level, they exhibit an effectively infinite molecular weight, with polymer chains covalently bonded into a rigid, densely cross-linked structure. As a result, thermosets are hard, infusible, and insoluble in most organic solvents, with only a small sol fraction potentially dissolving while the gel fraction can only swell. (14)

Above the glass transition temperature (Tg), thermosets become softer but never flow due to the permanent network structure. Below Tg, they exhibit high stiffness, strength, and hardness, while above Tg they display a rubbery plateau until thermal degradation occurs. Owing to their superior mechanical and thermal stability, thermosets are widely used in applications requiring high performance and dimensional stability at elevated temperatures. However, their permanent cross-linked structure prevents reshaping, reprocessing, and recycling, making them among the most difficult polymers to recycle and posing significant environmental challenges. (14)

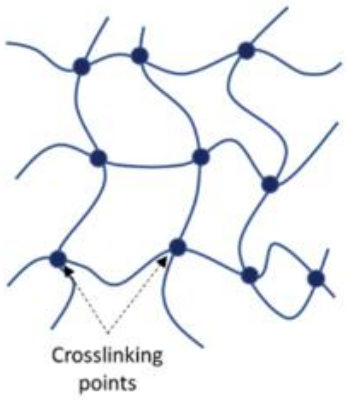

Figure 8 - Schematic representation of a thermosetting polymer after crosslinking.

To address the intrinsic trade-off between mechanical performance and recyclability, a new class of polymeric materials known as covalent adaptable networks (CANs) has been developed. CANs are cross-linked polymer networks containing dynamic covalent bonds that can reversibly break and reform in response to external stimuli such as heat or light.(15)

Figure 9 - Schematic illustration of the Covalent Adaptable Network (CAN) concept, combining the reprocessability of thermoplastics with the mechanical robustness of thermosets.

This dynamic behaviour enables a unique combination of properties: mechanical robustness and dimensional stability at service conditions, similar to thermosets, together with reprocessability and recyclability under appropriate activation, as observed in thermoplastics.

This unique combination arises from the dual nature of their network architecture. On one hand, covalent crosslinks provide mechanical robustness and chemical stability comparable to conventional thermosetting polymers; on the other hand, the presence of dynamic covalent bonds introduces reversibility into the network, allowing bond exchange reactions that enable reshaping, reprocessing, and recycling of the material (15).

Covalent adaptable networks (CANs) are cross-linked polymer networks containing dynamic covalent bonds capable of exchanging and reorganizing while partially preserving the network structure. Three main bond exchange mechanisms are typically identified: associative exchange, dissociative exchange, and metathesis. In many cases, these mechanisms may coexist or depend on factors such as bond energy, excess functional groups, or the presence of catalysts.

In associative systems, also referred to as vitrimers, bond formation precedes bond cleavage, maintaining a constant crosslink density. Typical examples include epoxy-based systems undergoing transesterification reactions catalyzed by Lewis acids or tertiary amines, as well as related exchange reactions such as transcarbonation, transcarbamoylation, transacetalization, and transamination, including systems involving boronic esters and silyl ethers.

In metathesis-based CANs, bond breaking and bond formation occur simultaneously, also preserving the overall network connectivity. Representative examples include acetal and boronic ester chemistries.

In dissociative CANs, bond cleavage occurs prior to bond reformation, leading to a temporary reduction in crosslink density and a marked decrease in viscosity upon heating. A well-known example is the reversible Diels–Alder reaction (e.g., furan–maleimide systems), in which elevated temperatures favor retro-Diels–Alder dissociation.

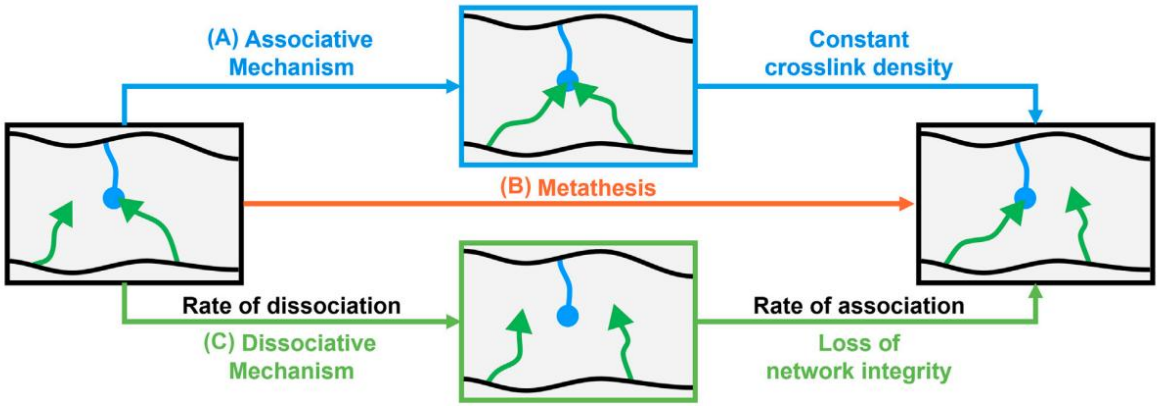

Figure 10 - Overview of the most common dynamic covalent bonds employed in renewable-based CANs.

Depending on the balance between bond breaking and reforming, partial network integrity may be retained, resulting in vitrimer-like behaviour, as observed for instance in disulfide-containing systems.

In CANs, the transition between solid-like and fluid-like behaviour is not defined by a sharp melting point but is conventionally associated with a viscosity of approximately 10^{12} Pa·s. Their viscoelastic response is typically investigated through stress relaxation experiments, where the decay of internal stress under constant deformation is monitored.

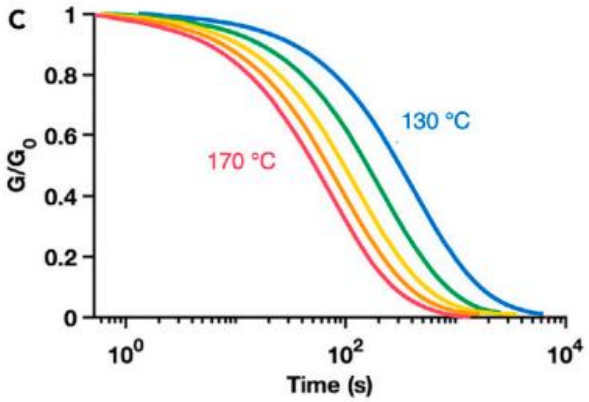

Figure 11 - Normalized stress relaxation curves obtained by rheological analysis at temperatures ranging from 130 °C to 170 °C

This behaviour originates from thermally activated bond exchange reactions, which allow network rearrangement and enable additional functionalities such as shape-memory behaviour, where deformation-induced stress can be relaxed upon heating, leading to recovery of the original shape. (14)

In vitrimer systems, stress relaxation is governed by the kinetics of bond exchange above the characteristic topology freezing temperature (Tv). The temperature dependence of the exchange rate follows Arrhenius behaviour, where the rate constant increases exponentially with temperature as a function of the activation energy.

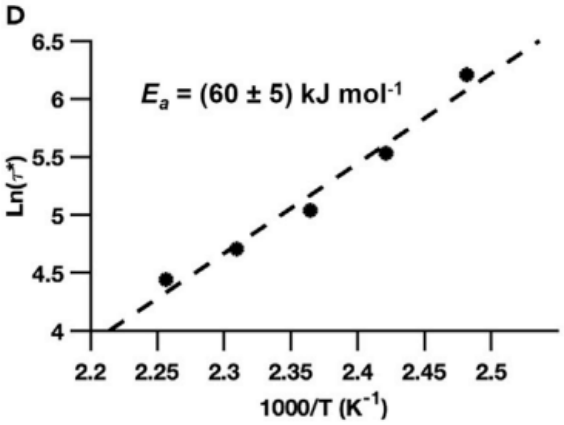

Figure 12 - Arrhenius representation of the characteristic relaxation time (τ) versus inverse temperature (1/T), used to determine the activation energy associated with bond exchange reactions. Adapted with permission from Elling and Dichtel.[68] Copyright © 2020 A

Linearization of the Arrhenius equation allows the determination of the activation energy for bond exchange, which directly influences the temperature required for effective network rearrangement and thus the processability of the material. (15)

Subsequently, transesterification and disulfide exchange will be specifically discussed, as they are the main mechanisms governing the ECO and DGEVA systems analysed in this thesis work.

1.3.1 Transesterification

Among the various dynamic covalent reactions investigated for the development of covalent adaptable networks (CANs), transesterification has received particular attention. Notably, the first vitrimer system reported by Ludwik Leibler in 2011 was based on this exchange mechanism (14). Transesterification is the exchange reaction between an ester and an alcohol, resulting in the formation of a new ester and a new alcohol (Figure 13).

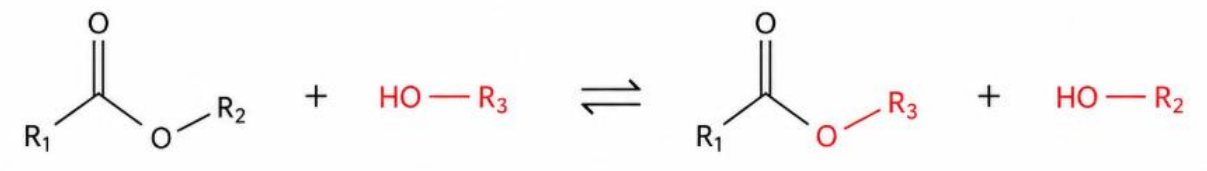

Figure 13 - General schematic representation of a transesterification reaction between an ester and a hydroxyl group (14)

This reaction can be catalyzed by strong acids, strong bases, or suitable enzymatic catalysts. Early studies demonstrated that the kinetics of dynamic bond exchange in epoxy-based vitrimers can be effectively tuned through the choice and concentration of the catalyst. In particular, increasing the catalyst concentration accelerates the transesterification rate without significantly affecting the activation energy, whereas modifications in catalyst structure influence both the reaction kinetics and the activation energy of the dynamic process. (16)(17)

In the present work, formulations based on epoxidized castor oil (ECO) were investigated. ECO is particularly suitable for vitrimeric applications because its molecular structure inherently contains both ester and hydroxyl functionalities, which are required for transesterification reactions. To promote dynamic bond exchange, dibutyl phosphate (DBP) was incorporated into the resin formulation as a transesterification catalyst. DBP acts as a Brønsted acid through its acidic hydroxyl group, facilitating the exchange reactions within the polymer network.

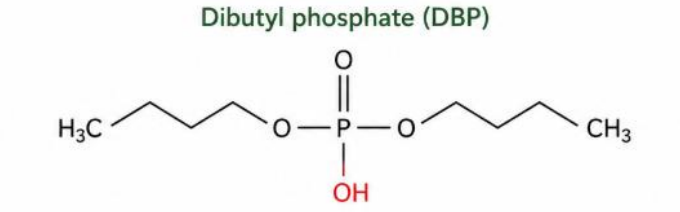

Figure 14 - Chemical structure of dibutyl phosphate (DBP), the transesterification catalyst employed in this work

The acid-catalyzed transesterification mechanism begins with the protonation of the ester carbonyl group by the catalyst, increasing the electrophilicity of the carbonyl carbon. This activation promotes the nucleophilic attack of a hydroxyl group, leading to the formation of a tetrahedral intermediate. Subsequently, proton transfer and rearrangement steps occur, allowing the original alkoxy group to leave and generating a new alcohol molecule. The resulting ester is finally deprotonated, regenerating the catalyst and completing the catalytic cycle. A schematic representation of this mechanism is shown in Figure 15.

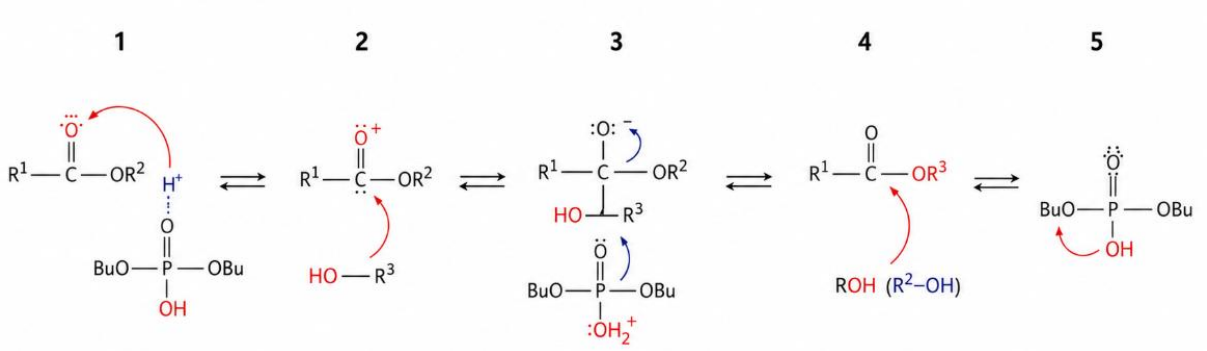

Figure 15 - Schematic representation of the transesterification reaction occurring between ester and hydroxyl groups present in the epoxidized oils used in this work, catalyzed by dibutyl phosphate (DBP) at elevated temperatures.

1) Protonation of the ester carbonyl: the dibutyl phosphate (DBP) catalyst protonates the carbonyl oxygen of the ester group, increasing the electrophilicity of the carbonyl carbon and activating it toward nucleophilic attack.

2) Nucleophilic attack by a hydroxyl group: a hydroxyl group belonging to another ECO chain attacks the activated carbonyl carbon, initiating the transesterification reaction.

3) Formation of the tetrahedral intermediate: the nucleophilic attack leads to the formation of a tetrahedral intermediate, in which the carbonyl carbon is temporarily bonded to both the incoming hydroxyl group and the original alkoxy group.

4) Exchange and leaving group departure: proton transfer and rearrangement within the tetrahedral intermediate promote the departure of the original alkoxy group, resulting in the formation of a new ester bond and the release of an alcohol molecule.

5) Deprotonation and catalyst regeneration: the newly formed ester undergoes deprotonation, restoring the neutral product and regenerating the DBP catalyst, which can participate in further transesterification reactions.

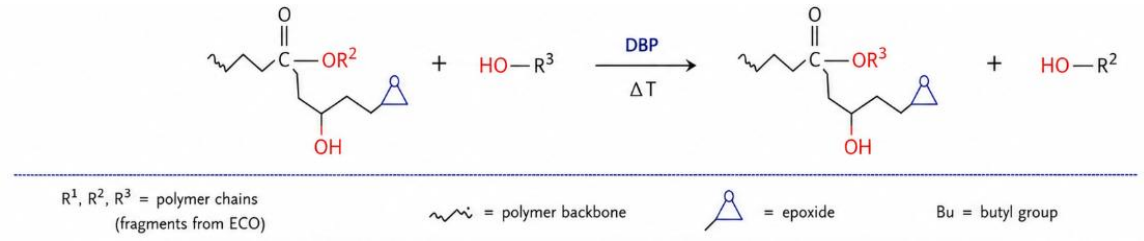

Figure 16 - Overall schematic representation of the DBP-catalyzed transesterification process occurring in the ECO network.

Because the reaction proceeds through the formation of a relatively stable tetrahedral intermediate before bond cleavage occurs, transesterification is classified as a stepwise associative exchange mechanism. As a consequence, network rearrangement can take place while maintaining the overall crosslink density, which is the characteristic feature of vitrimeric materials.

Following the pioneering work on transesterification-based vitrimers, numerous CAN systems have been developed exploiting this dynamic chemistry. Among them, epoxy resins have attracted considerable interest due to their wide range of applications, including coatings, adhesives, electronic devices, composite materials, and LED encapsulation systems (17).

1.3.2 Disulfide exchange

Disulfide exchange reactions represent another of the most widely studied dynamic covalent chemistries for the development of covalent adaptable networks (CANs). The reversible nature of disulfide bonds enables polymer networks to undergo bond rearrangement under appropriate stimuli, providing materials with healing, reprocessing, recycling, and stress-relaxation capabilities.

In aromatic disulfide-containing epoxy networks such as DGEVA, the predominant rearrangement pathway is generally attributed to direct disulfide–disulfide exchange. This mechanism can occur without the addition of catalysts or external reagents, allowing efficient network rearrangement at elevated temperatures while preserving the crosslinked structure. (18)

The use of sulfur-containing dynamic bonds was first investigated by Tobolsky and co-workers in the 1960s, who demonstrated that disulfide exchange reactions could induce stress relaxation in vulcanized rubber networks. Later, Tesoro et al.(19) extended this concept to thermosetting epoxy resins, showing that the reversible cleavage and reformation of disulfide bonds allowed the production of degradable and reprocessable thermosets. (14,20)

Compared with other vitrimeric systems based on transesterification or transamination reactions, disulfide-containing networks offer several advantages, including excellent mechanical performance, catalyst-free bond exchange, ease of processing, scalability, and relatively simple synthetic routes (21). The dynamic nature of the S–S bond allows the network topology to rearrange through disulfide exchange reactions when exposed to external stimuli, typically heat, while maintaining the overall crosslinked structure. In addition, disulfide bonds can undergo cleavage in the presence of suitable solvents or reducing agents, enabling chemical recycling and network degradation. (22,23)

In epoxy-based CANs, one of the most widely used curing agents for introducing dynamic disulfide functionalities is 4-aminophenyl disulfide (4-AFD) (24,25). Owing to the presence of both aromatic amine groups and a central disulfide linkage, 4-AFD can simultaneously participate in the epoxy curing reaction and provide dynamic exchangeable bonds within the resulting network. In the present work, a bio-based epoxy resin derived from vanillin (DGEVA) was cured using 4-AFD, generating a crosslinked network capable of undergoing thermally activated disulfide exchange reactions.

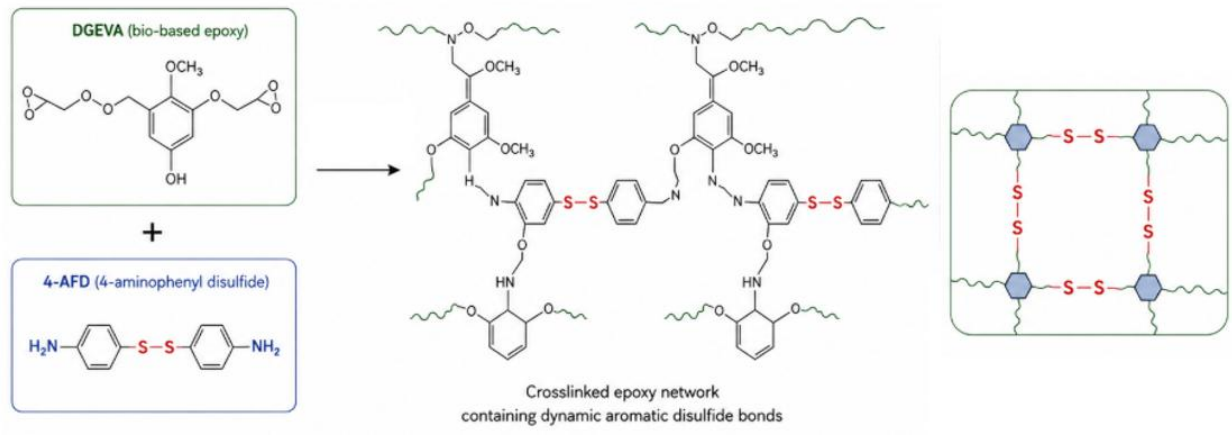

Figure 17 - Schematic illustration of the DGEVA/4-AFD curing process and the resulting crosslinked epoxy network containing dynamic aromatic disulfide linkages.

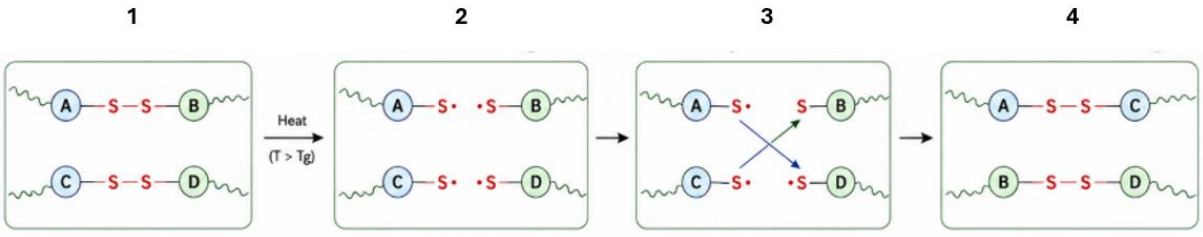

Figure 18 - Schematic representation of the disulfide exchange mechanism in the DGEVA/4-AFD vitrimer network.

1) Initial network: polymer chains are connected through aromatic disulfide bonds (S–S).

2) Bond activation: upon heating, the dynamic disulfide bonds become activated and temporarily dissociate.

3) Exchange reaction: the sulfur species recombine with neighboring chains, forming new disulfide bonds.

4) Rearranged network: the network topology changes while maintaining the overall crosslink density.

These dynamic bond rearrangements are responsible for the stress-relaxation, reprocessing, and healing behaviour exhibited by the material, which were further investigated through thermal, mechanical, and healing experiments presented in the following sections.

1.4 Conductive polymers

The intrinsic electrical insulating properties of polymers have led to their widespread use in electrical and electronic applications, with typical electrical resistivities on the order of 10^{15} Ω·m. Nevertheless, considerable research efforts have been devoted to imparting electrical conductivity to polymeric materials by incorporating conductive fillers such as carbon black, carbon fibers, metallic particles, or intrinsically conductive polymers. As a result, a

broad class of materials known as electrically conductive polymer composites (CPCs) has emerged since the 1950s (26).

These composites exhibit electrical resistivities intermediate between those of metallic conductors (approximately 10^{-7} Ω·m) and conventional insulating polymers (27), enabling their use in a wide range of applications. Typical examples include floor-heating systems, electronic devices (28), electromagnetic interference (EMI) shielding materials, and antistatic components based on semiconductive materials. More recently, conductive polymer composites have also attracted significant interest for sensing and monitoring applications (29).

Compared with conventional metallic conductors, conductive polymer composites offer several advantages, including low density, ease of processing and shaping, corrosion resistance, and the possibility of tailoring their electrical conductivity over a broad range by controlling the type and concentration of the conductive filler (29).

The electrical conductivity of polymer composites is commonly described through the concept of the percolation threshold. This parameter represents the minimum concentration of conductive filler required to form a continuous and interconnected conductive network within an insulating polymer matrix. Below the percolation threshold, the conductive particles remain isolated and the composite behaves as an electrical insulator.

Several factors influence the percolation threshold of conductive polymer composites:

Polymer Polarity

One of the most important is the nature of the polymer matrix. In particular, polymer polarity has been reported to affect the critical filler concentration required to establish a conductive network. Miyasaka et al. (28) observed that polymers with higher polarity and surface tension generally exhibit higher percolation thresholds, indicating that a larger amount of conductive filler is required to achieve electrical conductivity.

Viscosity

The viscosity of the polymer matrix is another key parameter affecting the formation of conductive pathways (30,31). Higher polymer viscosities lead to increased shear forces during processing, which can damage the structure of conductive fillers and hinder the development of a continuous conductive network. As a result, the percolation threshold is shifted toward higher filler concentrations. This effect is particularly relevant for carbon

fiber-filled systems, where excessive shear can reduce the fiber aspect ratio and limit the formation of three-dimensional conductive networks (30).

Physical characteristics of the conductive filler

The physical characteristics of the conductive filler also play a crucial role. For carbon fibers, electrical conductivity strongly depends on the fiber aspect ratio, with longer and thinner fibers generally providing lower percolation thresholds and higher conductivity. However, achieving a homogeneous dispersion of the fibers within the polymer matrix often requires significant shear during processing, which may reduce the aspect ratio through fiber breakage. Therefore, an optimal balance between filler dispersion and preservation of fiber morphology is essential for maximizing the electrical performance of conductive composites (32).

Temperature effect

Temperature effects also play a significant role in the electrical behavior of conductive polymer composites. The dependence of resistivity on temperature is a widespread but complex phenomenon that has been extensively investigated. Based on the rate at which resistivity increases with temperature, this behavior can be broadly classified into two categories: gradual variation and abrupt variation. Gradual changes are typically associated with thermal expansion of the polymer matrix, which increases the distance between conductive fillers and slightly disrupts conductive pathways. In contrast, abrupt changes are often linked to phase transitions of the polymer, such as melting or glass transition, which can significantly alter the microstructure and lead to a sharp increase in resistivity.

Effects of polymer matrix

Although the electrical conductivity of polymer composites is influenced by the nature of the polymer matrix, establishing a universal relationship between polymer type and electrical resistivity remains challenging. This is because conductivity is affected by several interconnected factors, including the formulation composition, processing conditions, filler concentration, and filler dispersion within the matrix (26). Furthermore, the same conductive filler may exhibit different behaviours depending on the polymer used, while deformation and thermal treatments can further alter the electrical response of the material. Consequently, it is difficult to draw general conclusions regarding the effect of the polymer matrix on conductivity, as the electrical performance of conductive composites strongly depends on the specific filler–polymer system under investigation (26).

1.5 Applications

This study is not directly aimed at the development of a commercial material, but rather is proposed as a preliminary investigation of biobased polymers reinforced with carbon fibers.

In recent years, the application of such materials in multifunctional coatings has attracted increasing attention, as they can exhibit excellent surface properties, including high corrosion resistance (33) and the ability to act as barriers against bacterial activity (34,35).

In this context, there is also growing interest in the development of polymer coatings based on the incorporation of different types of fillers. In particular, it is well established that the addition of conductive fibers can significantly enhance electrical properties by several orders of magnitude. This improvement in electrical conductivity enables the development of polymer-based coatings for a wide range of applications, including electromagnetic interference shielding (36), sensing applications (37), and anti-icing systems (38). Among these, anti-icing applications are particularly relevant, as they can prevent ice formation and improve performance in systems such as aerodynamic surfaces. For instance, wind turbine blades may suffer damage or reduced energy production when ice accumulates on their surfaces, a common issue in turbines operating in cold climates (39). The anti-icing functionality is typically based on Joule heating of carbon fiber-reinforced polymer coatings. More specifically, the heat generated, Q, over a time interval t, can be estimated using the well-known Joule's law (1.5.1):

$$Q = V * i * t \tag{1.5.1}$$

where V and I represent the applied voltage and the current flowing through the composite, respectively.

2. Materials and Methods

2.1 ECO

Epoxidized castor oil (ECO) was achieved by epoxidizing castor following a procedure shown un Figure 20.

Castor oil (CO) was purchased from Mundo dos Óleos (Brasília, Brazil). The catalyst Amberlite™ IR-120, glacial acetic acid (≥99), hydrogen peroxide (50%, H_2O_2), magnesium sulfate (≥99.5%), ethyl acetate, and deuterated chloroform ($CDCl_3$, 99.8% D) were acquired from Sigma-Aldrich (São Paulo, Brazil).
The chemical structure of ECO is represented in Figure 19.

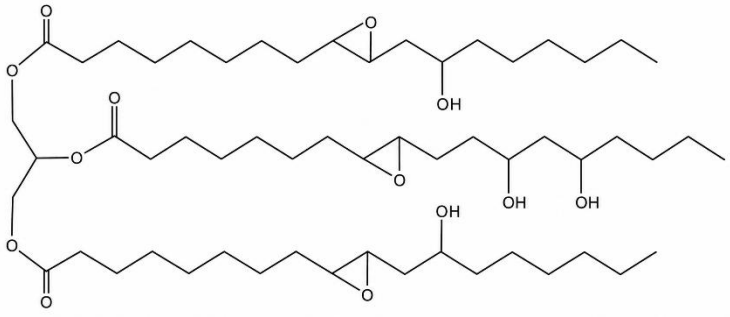

Figure 19 - ECO molecular structure

Triarylsulfonium hexafluoroantimonate salt acts as a cationic photoinitiator. Upon UV irradiation, it generates a strong Brønsted acid that initiates the cationic ring-opening polymerization of epoxy groups, leading to the formation of a crosslinked thermoset network.

Isopropylthioxanthone (ITX) used as photosensitizer to enhance the efficiency of the cationic photoinitiating system. Upon UV irradiation, ITX absorbs light and transfers energy or electrons to the triarylsulfonium salt, promoting acid generation and consequently accelerating the cationic ring-opening polymerization of epoxy groups. It is a mixture of isomers 2 and 4, synthesized by Sigma-Aldrich (Milan, Italy).

Dibutyl phosphate (DBP) was used as a transesterification catalyst to impart covalent adaptable network (CAN) behavior. At elevated temperatures, DBP catalyzes ester–hydroxyl exchange reactions, enabling bond rearrangement within the crosslinked network while preserving the overall crosslink density. This dynamic bond exchange allows stress relaxation, reshaping, welding, and reprocessing of the material

The chemical structure of all the components are showed in the Figure 20 below.

Figure 20 - Structural formulas of the components employed in the ECO-based formulation

2.2 DGEVA

Diglycidyletether of vanillyl alcohol (DGEVA) (EEW=139 g(eq), synthesized by Specific Polymers through a two-step procedure from vanillin and epichlorohydrin. The general chemical structure of DGEVA is reported in Figure 21.

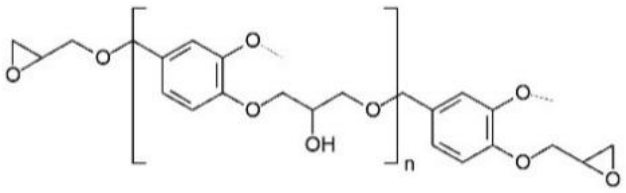

Figure 21 - Diglycidylether of vanillyl alcohol chemical structure

As thermal hardener 4,4'-aminophenyl disulfide (4AFD) (AHEW=62 g/eq) was purchased from Sigma-Aldrich. The chemical structure of 4AFD is shown in Figure 22.

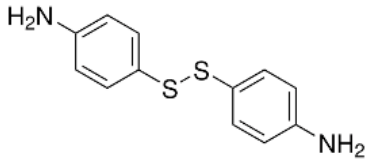

Figure 22 - 4-Aminophenyl disulfide chemical structure

The epoxy network formed between diglycidyl ether of vanillyl alcohol (DGEVA) and 4,4'-aminophenyl disulfide (4AFD) exhibits vitrimer-like behaviour due to the presence of dynamic disulfide bonds within the crosslinked structure. Upon thermal activation, disulfide exchange reactions occur through radical-mediated and associative mechanisms, enabling reversible network topology rearrangement while preserving crosslink density. This dynamic bond exchange imparts stress relaxation, reprocessability, and shape adaptability to the thermoset material.

2.3 Recycling Carbon Fiber

Additionally, recycled carbon fibres (RCF), with a length of 2 mm, were introduced in different amounts. RCF were recovered from dismissed composites via chemical recycling. SEM image of the filler is reported in Figure 23.

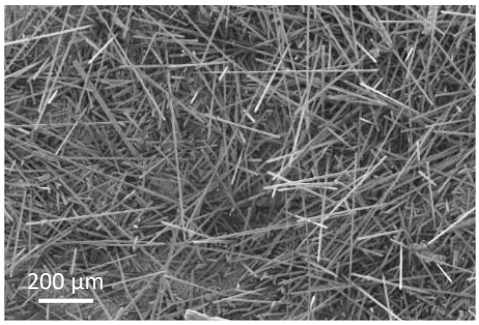

Figure 23 - SEM image of RCF

The recycling methodology adopted in this work is based on the mechanical recovery of carbon fibers from expired prepreg materials, following an approach developed by Universidad Rey Juan Carlos for multifunctional composite applications (40).

Initially, the prepreg waste was subjected to multiple acetone washing cycles in order to remove residual epoxy resin that had not completely reacted during the original curing process. This cleaning step is essential to reduce the presence of polymeric residues on the fiber surface and improve the subsequent dispersion and interfacial behaviour of the recycled fibers.

After the solvent-cleaning stage, the recovered material was mechanically processed using a milling procedure performed at 3000 rpm with a 2 mm sieve. To ensure homogeneous fragmentation and improve process reproducibility, the material underwent 10 consecutive milling cycles. This treatment generated a heterogeneous population of recycled carbon fibers characterized by different fiber lengths.

The resulting fiber morphology was then evaluated through polydispersity analysis, which represents a key parameter for assessing the quality and uniformity of the recycled material. Lower polydispersity values indicate a more homogeneous fiber population and therefore better process control and reproducibility.

The obtained recycled fibers can subsequently be incorporated into polymeric matrices for the development of multifunctional composites with enhanced mechanical, electrical, and thermal properties.

2.4 Formulations preparation

For each matrix type, three different formulations were prepared: a pristine formulation without filler, and formulations containing 10 phr and 20 phr of recycled carbon fibers.

Regarding ECO: in each formulation, 2 phr of cationic photoinitiator, Triarylsulfonium hexafluoroantimonate salts, 2 phr of photosensitizer, Isopropylthioxanthone (ITX), and 15 phr of transesterificator catalyst, dibutyl phosphate, were added to epoxidized castor oil (ECO). Afterward, a THINKYMIXER ARE-250 planetary mixer was used to homogeneously distribute fillers in the monomer and degas the formulations, according to the following program: 1 min mixing and then 1 min degassing at 1600 rpm, 1 min mixing and then 1 min degassing at 1800 rpm, and finally 2 min mixing at 2000 rpm.

Formulation	RCF (phr)	RCF (%wt)	PI (phr)	ITX (phr)	DBP (phr)
ECO Pristine	-	-	2	2	15
ECO, 10 phr RCF	10	9.09			
ECO, 20 phr RCF	20	16.67			

Table 1 - Components for each formulation

For the DGEVA system, all formulations were prepared using a stoichiometric excess of the disulfide-containing curing agent in order to promote efficient dynamic bond exchange and enhance the network rearrangement capability. Specifically, 1.2 equivalents of 4-aminophenyl disulfide (4AFD), corresponding to 53.5 phr, were employed. The required amount of hardener was calculated from the epoxide equivalent weight (EEW) of the resin and the amine hydrogen equivalent weight (AHEW) of the curing agent according to Equation 2.1(41,42).

$$phr = \frac{1.2 \times AHEW}{EEW} \times 100 \quad (2.1)$$

Prior to the addition of the curing agent and recycled carbon fibers (RCF), the DGEVA resin was heated at 100 °C for 10 min to reduce its viscosity and facilitate subsequent processing. The hardener and fillers were then incorporated into the resin, and the resulting mixture was homogenized and degassed using a planetary centrifugal mixer (THINKY ARE-250).

The mixing procedure consisted of a multi-step sequence comprising alternating mixing and degassing stages of 1 min each at 1600 rpm and 1800 rpm, followed by a final homogenization step of 2 min at 2000 rpm. This protocol enabled efficient filler dispersion while minimizing air entrapment, resulting in homogeneous and void-free formulations characterized by a uniform distribution of the recycled carbon fibers throughout the bio-based epoxy matrix.

Formulation	RCF (phr)	4AFD (phr)
DGEVA Pristine	-	53,3
DGEVA, 10 phr RCF	10	
DGEVA, 20 phr RCF	20	

Table 2 - components for each formulation

2.5 Characterization of curing process

2.5.1 Fourier Transform Infrared Spectroscopy in transmission mode (FT-IR)

The following analyses were carried out on both the UV-cured ECO formulations and the thermally cured DGEVA systems. Common parameters and calculation methods are described below, while the specific experimental conditions adopted for each system are reported separately.

Fourier Transform Infrared Spectroscopy (FT-IR) was used to investigate the cross-linking process with a Thermo Scientific Nicolet iS50 spectrometer (Thermo Fisher Scientific, Norwalk, CT, USA). Spectra were acquired at a resolution of 4 cm^{-1}, and the data were processed using OMNIC software (Thermo Fisher Scientific). The conversion was calculated using Equation 2.2:

$$Conversion\ (\%) = \frac{\left(\frac{A_{fun}}{A_{ref}}\right)_{t=0} - \left(\frac{A_{fun}}{A_{ref}}\right)_{t}}{\left(\frac{A_{fun}}{A_{ref}}\right)_{t=0}} \cdot 100 \qquad (2.2)$$

For the ECO-based formulations, the liquid samples were manually deposited onto a SiC substrate using a film applicator bar, resulting in coatings approximately 12 μm thick. The films were then irradiated with a DMAX lamp under curing conditions corresponding to an irradiance of 177 mW/cm², achieved by positioning the samples at a distance of 14 cm from the lamp source.

The photocuring reaction was monitored by tracking the decrease of the oxirane ring absorption band in the 825–840 cm^{-1} region, while the peak at 1727 cm^{-1}, associated with the carboxylic group and considered invariant during the reaction, was used as an internal reference.

According to Equation 2.2: A_{fun} corresponds to the area of the functional group peak (the acrylate band at 810 cm^{-1}), and A_{ref} corresponds to the reference peak at 1727 cm^{-1}. Spectra were recorded at different irradiation times to follow the progress of the reaction.

For the DGEVA systems, thermal curing was performed using an ArgoLab TCN30 Plus oven. The formulations were deposited onto silicon substrates with the aid of a spreader bar, producing films with an average thickness of about 12 μm. The infrared spectrum of each sample was initially acquired prior to the thermal treatment (pre-curing, $t = 0$ min). Subsequently, the films were cured at 150 °C for 1 h, followed by a post-curing step at 200 °C for an additional hour. After the curing process, IR spectra were collected again. The conversion percentage of the samples was then calculated according to Equation 2.2.

Specifically, A_{fun} corresponds to the integrated area of the asymmetric epoxide C–O–C stretching band (950–810 cm^{-1}) and the symmetric C–O–C vibration band (880–750 cm^{-1}). The obtained values were normalized with respect to A_{ref}, associated with the carbonyl stretching region in the 1780–1680 cm^{-1} range [60]. The terms $t = 0$ and t indicate the spectra collected before and after thermal treatment, respectively.

2.5.2 Photo-differential scanning calorimetry (photo-DSC)

Photo-differential scanning calorimetry (Photo-DSC) was performed on the ECO formulations to further investigate the photocuring behaviour and validate the conversion values obtained by FTIR analysis. (43) The experiments were carried out using a Mettler Toledo DSC-1 calorimeter equipped with a GC100 Gas Controller. This technique allows the simultaneous evaluation of the reaction kinetics and the heat released during the UV-induced crosslinking process.

For each measurement, approximately 5–15 mg of liquid formulation was placed in a 40 μL aluminium crucible, while an empty crucible was used as the reference. The analysis was conducted at constant temperature (100°C), in N2 controlled atmosphere (40 ml/min) and for the irradiation of the samples was used a Hamamatsu LC8 mercury lamp (Hamamatsu Photonics) at 100% of the intensity. Irradiation was provided by a Hamamatsu LC8 mercury lamp (Hamamatsu Photonics) operating at full intensity.

Each experiment consisted of two consecutive stages: an initial dark period of 2 min, during which the lamp remained switched off, followed by 3 min of UV irradiation. Subsequently, a second run was performed to establish the baseline and ensure complete curing of the sample. The final photopolymerization signal was obtained by subtracting the second thermogram from the first, thus isolating the heat flow associated exclusively with the photocrosslinking reaction(44).

2.5.3 Dynamic and isothermal DSC

Dynamic and isothermal DSC analyses were carried out on the DGEVA formulations using a Mettler Toledo DSC-1 calorimeter under a nitrogen atmosphere with a constant flow rate of 40 mL min^{-1}. For each formulation, three independent measurements were performed and the reported values correspond to the average results, including the associated standard deviations. Approximately 5–10 mg of uncured resin were placed in a 40 μL aluminium crucible, while an empty crucible was used as the reference.

Dynamic DSC experiments were conducted from 25 to 300 °C at a heating rate of 3 K min^{-1} in order to investigate the curing behaviour of the formulations. The heat flow was continuously monitored as a function of temperature and time. The temperature corresponding to the maximum of the exothermic peak (T peak) was used as an indicator of the curing rate, whereas the onset (T onset) and endset (T endset) temperatures were used to define the processing window and the thermal conditions required to achieve complete network formation.

Based on the results of the dynamic scans, isothermal DSC measurements were subsequently performed at 200 °C. This temperature was selected to monitor the evolution of the curing process under constant thermal conditions, allowing a direct comparison of the reaction kinetics among the different formulations. The experimental curing enthalpy (ΔH exp) was determined by integrating the exothermic heat flow associated with the polymerization reaction.

DSC analysis was also employed to determine the glass transition temperature (Tg) of the cured materials. The Tg was identified as the inflection point of the baseline shift associated with the change in heat capacity, corresponding to the maximum of the first derivative of

the heat flow signal. These measurements were performed between 0 and 200 °C at a heating rate of 2 K min^{-1}.

2.5.4.1 Conversion and kinetics calculations

The kinetic parameters and conversion degree for both ECO and DGEVA systems were calculated using the same theoretical framework.

The polymerization rate (Rp) was determined according to Equation (2.3): (45)

$$R_p = \frac{1}{\Delta H_{tot}} \cdot \left(\frac{dH}{dt}\right)_T \tag{2.3}$$

where Rp is the polymerization rate [s^{-1}], ΔH tot is the total enthalpy released upon complete cross-linking [J/g], and (dH/dt) T is the heat flow measured under isothermal conditions [J/(g·s)].

The total enthalpy ΔH tot was calculated as: (45)

$$\Delta H_{tot} = n \cdot f \cdot H_{ep} \cdot \frac{1}{PM} \tag{2.4}$$

where:

- n is the number of epoxy groups per mole of monomer
- f is the fraction of epoxy groups contributing to network formation (f = 1 in this work)
- H ep is the theoretical enthalpy of epoxy ring opening (74,000 J/mol, exothermic)
- PM is the molecular weight of the monomer (975 g/mol for ECO and 266.29 g/mol for DGEVA)

The conversion degree (C) was obtained by integration of Equation 2.5, according to (45):

$$C = \frac{1}{\Delta H_{tot}} \int_0^t \left(\frac{dH}{dt}\right)_T dt \tag{2.5}$$

2.5.4 Rheology

Rheological characterization was performed to evaluate the viscosity behaviour of the prepared formulations as a function of fiber content and to assess the quality of fiber dispersion within the two investigated resin matrices. The measurements were carried out

using an Anton Paar MCR 302e™ rotational rheometer equipped with a parallel-plate geometry.

Two parallel plates with a diameter of 25 mm were employed, maintaining a 0.5 mm gap between them. The analyses were conducted at the same temperatures used during the mixing process, namely 25 °C for the ECO system and 45 °C for the DGEVA system. The higher testing temperature adopted for DGEVA was necessary to prevent crystallization at room temperature and to ensure adequate processability and homogeneous fiber dispersion during mixing.

For each measurement, a sufficient amount of uncured resin formulation was placed between the plates to completely fill the testing gap. The viscosity was then recorded over a shear rate range from 0.01 to 100 s^{-1}. The rheological behaviour of each formulation was subsequently represented by plotting viscosity (Pa·s) as a function of shear rate (s^{-1}), allowing the influence of fiber loading and matrix type on the flow properties of the systems to be evaluated.

2.6 Characterization of the cured samples

2.6.1 DMTA

Dynamic Mechanical Thermal Analysis (DMTA) was employed to investigate the viscoelastic properties of the crosslinked polymers from both ECO and DGEVA formulations. When a polymeric material is subjected to a sinusoidal deformation, its response is composed of an elastic contribution (storage modulus, E') and a viscous contribution (loss modulus, E''). The ratio between these parameters defines the damping factor, tan (δ), which represents the energy dissipated as heat during each deformation cycle (46).

Measurements were performed using a Triton Technology Tritec 2000 instrument operating in tensile (uniaxial) oscillatory mode at a frequency of 1 Hz. Samples were prepared by casting the formulations into silicone molds, obtaining specimens with average dimensions of 0.5 × 3.5 × 13 mm. The materials were then photocured using a DYMAX ECE Flood Lamp with an intensity of 150 mW/cm² for 120 s per side.

For ECO formulations, the thermal program consisted of cooling the chamber to −60 °C using liquid nitrogen, followed by heating to 100 °C at a rate of 3 °C/min. For DGEVA formulations, measurements were performed over an extended temperature range, from 0 °C up to 200 °C, maintaining the same heating rate of 3 K/min.

During both analyses, the storage modulus (E'), loss modulus (E''), and damping factor tan(δ) were continuously recorded as a function of temperature. The glass transition temperature (Tg) was determined from the maximum of the tan(δ) peak.

The crosslinking density ν_c [mol/m³] was calculated using the following equation (47):

$$\nu_c = \frac{E'}{3RT} \tag{2.6}$$

where E' is the storage modulus in the rubbery plateau region, measured at T = Tg + 50 °C (in Kelvin), R is the universal gas constant (8.314 J·mol⁻¹·K⁻¹), and T is the absolute temperature.

Although thermal degradation was not directly quantified by DMTA, differences in high-temperature mechanical stability between ECO and DGEVA formulations could be qualitatively assessed through the evolution of the storage modulus at elevated temperatures, particularly in the region approaching the onset of thermal breakdown.

2.6.2 TGA

Thermogravimetric analysis (TGA) is a technique that continuously monitors the mass variation of a sample subjected to a controlled heating program, enabling the investigation of its thermal degradation behaviour. The analysis was carried out using the same methodology for both ECO- and DGEVA-based formulations. (48)

The measurements were performed using a Mettler Toledo TGA/SDTA 851e™ instrument. Samples were heated in air from 25 °C to 900 °C at a constant heating rate of 10 °C min⁻¹ under a continuous flow of dry air (40.0 mL/min).

Each sample consisted of a small fragment of photocured resin weighing a few milligrams. The specimen was placed in an alumina ceramic crucible, which was subsequently positioned on the high-precision balance of the instrument. The curing procedure adopted for the samples was identical to that described for the DMTA tests.

The resulting TGA profile was recorded as residual mass percentage (% wt) as a function of temperature (°C). The first derivative of the TGA curve yields the derivative thermogravimetric (DTG) curve, which represents the rate of mass loss (dm/dT) as a function of temperature. The DTG curve facilitates the identification of the thermal degradation processes occurring within the samples.

2.6.3 Stress relaxation analysis

Stress relaxation measurements were performed on UV-cured ECO samples and crosslinked DGEVA using an Anton Paar MCR 302e rheometer. Disc-shaped specimens with an approximate thickness of 1 mm were used; the diameter was 25 mm for both ECO and DGEVA samples.

Prior to testing, each specimen was subjected to a constant normal force to ensure proper contact between the plates and thermal equilibration: 1 N for ECO samples and 5 N for DGEVA samples, both applied for 15 min at the selected test temperature. A constant strain of 3% was then imposed, and the evolution of the relaxation modulus was recorded as a function of time.

Measurements were carried out at four different temperatures for each material. Specifically, ECO samples were tested at 70 °C, 80 °C, 90 °C, and 100 °C, while DGEVA samples were tested at 130 °C, 140 °C, 150 °C, and 160 °C.

The relaxation modulus, G(t), was normalized with respect to its initial value, G_0. The characteristic relaxation time (τ) was defined as the time required for the normalized modulus to decay to 1/e of its initial value (49), assuming an exponential decay behaviour described by:

$$G(t) = G_{t0} e^{-\frac{t}{\tau}} \tag{2.7}$$

The activation energy (E_a) was determined from the Arrhenius relationship:

$$\ln(\tau) = \ln(\tau_0) + E_a \frac{1000}{RT} \tag{2.8}$$

where E_a is the activation energy (J/mol), R is the universal gas constant (J/mol·K), T is the absolute temperature (K), and τ_0 is the pre-exponential factor. By plotting ln(τ) versus 1000/T, the activation energy was obtained from the slope (α) of the linear fit according to:

$$E_a = a \times 1000 \times R \tag{2.9}$$

2.6.4 Gel content

The gel content (%gel) was determined by evaluating the mass of the insoluble fraction remaining after solvent extraction. Cured specimens (approximately 200 mg) were immersed in chloroform for 24 h at room temperature to remove any soluble species, including unreacted monomers, oligomers, and non-crosslinked polymer fractions. Following extraction, the samples were first dried under ambient conditions for 24 h and

then further dried at 60 °C for 6 h to ensure complete evaporation of residual solvent before weighing.

The gel content was calculated as the ratio between the final dry mass after extraction (W_1) and the initial mass before extraction (W_0), according to Equation 2.10:

$$\%gel = \frac{W_1}{W_0} \times 100 \tag{2.10}$$

where W_0 is the initial mass of the cured specimen and W_1 is the mass of the insoluble residue after solvent extraction and drying. The gel fraction provides an indirect measure of the crosslinking extent and network integrity, with higher values indicating the formation of a more interconnected and solvent-resistant structure. All measurements were performed in triplicate for each formulation, and the reported values correspond to the average of the three determinations.

2.7 Functional physical tests

2.7.1 Electrical conductivity and joule heating measurements

Electrical conductivity and Joule heating analyses were performed for both ECO and DGEVA matrices using specimens with the same geometry adopted for DMTA and stress relaxation experiments. At least three measurements were carried out for each sample in order to ensure the reproducibility of the results.

Electrical conductivity measurements were conducted using a Keithley Instruments 2410 source meter. To reduce contact resistance, silver conductive paint was applied on two opposite faces of the specimens, while copper wires were attached to enable the electrical connection. The electrical resistance (R) was determined from the slope of the voltage–current (V–I) curve according to Ohm's law, by applying voltage sweeps from 0 V up to a maximum value selected depending on the resistivity of the material. Subsequently, the electrical conductivity (σ) was calculated according to the following relationship:

$$\sigma = \frac{L}{A \times R} \tag{2.10}$$

where L is the distance between the electrodes and A is the cross-sectional area of the specimen.

The Joule heating behaviour was evaluated using the same specimens and electrical setup adopted for the conductivity measurements. During the tests, voltages suitable for the resistivity range of each material were applied while monitoring the surface temperature with a FLIR Systems T530 thermal camera represented in Figure 24.

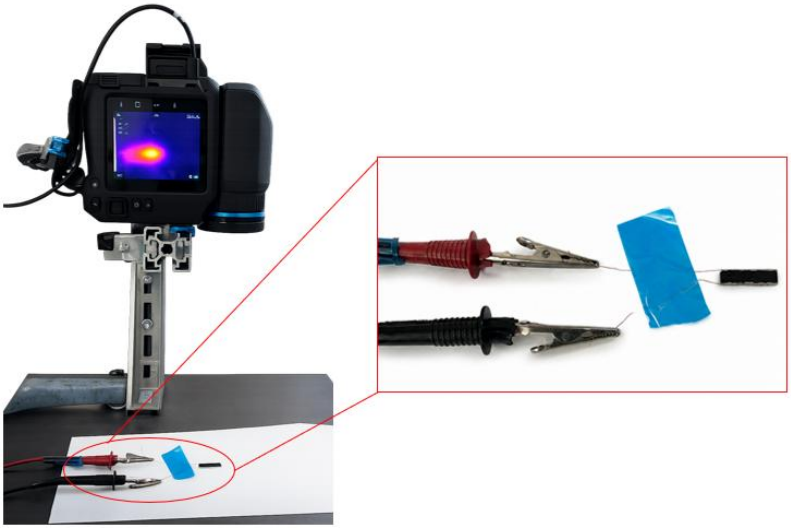

Figure 24 – setup for electrical conductivity and joule heating measurements

For each applied voltage, the maximum temperature (T_{max}) and the average temperature (T_{av}) were recorded after the system reached thermal stabilization. In order to ensure stable and reproducible thermal conditions, each experimental parameter was maintained for 5 minutes before the thermal measurements were acquired. In addition, the Joule heating homogeneity (H) was determined according to the following equation:

$$H = 1 - \frac{T_{max} - T_{av}}{T_{av}} \tag{2.11}$$

2.7.2 Tensile test

Mechanical characterization of both ECO and DGEVA matrices was performed through tensile tests conducted at room temperature using an MTS Systems Corporation QTest™/10 Elite universal testing machine. The experiments were carried out with a 5 kN load cell and a crosshead speed fixed at 2 mm/min in order to evaluate the bulk mechanical behaviour of the materials.

For each formulation, a minimum of five specimens was tested to guarantee the reproducibility of the experimental results. The mechanical properties were subsequently expressed as mean values accompanied by the related standard deviations.

2.7.3 Microstructural analysis

For both ECO and DGEVA matrices, scanning electron microscopy (SEM) and Field emission scanning electron microscopy FESEM analyses were performed to examine the dispersion of fillers within the polymeric matrix and to assess the interfacial adhesion between the formulated materials and the substrates. In particular, these analyses were used to evaluate the homogeneity of filler distribution and to identify any possible agglomerates or structural defects that could affect the final material properties.

Micrographs were collected for each sample using a JEOL Ltd. JCM-6000 PLUS scanning electron microscope and FESEM were taken with the ZEISS Supra 40 . Prior to imaging, the sample surfaces were coated with a thin conductive platinum layer, approximately 10 nm in thickness, in order to minimize charging effects during observation and to enhance image resolution.

2.7.4 Contact angle

The contact angles of all cured materials were measured using a Krüss DSA10 tensiometer (Krüss Scientific, Hamburg, Germany) equipped with a digital camera. A droplet of distilled water was placed on the surface of each sample, and ten optical scans were carried out in order to determine the contact angle between the droplet and the substrate. The measurements were performed in triplicate for both ECO and DGEVA samples, following the same experimental procedure.

2.7.5 Healing measurements

In the case of DGEVA, surface cracks were intentionally introduced onto the specimens previously employed for the DMTA analysis. Before crack generation, the sample surfaces were first levelled using a circular grinding machine with 800-grit abrasive paper in order to ensure a perfectly flat and uniform surface. Subsequently, cracks were created using a penetrating blade inclined at 45° with respect to the sample surface, producing defects with an approximate depth of 200 μm.

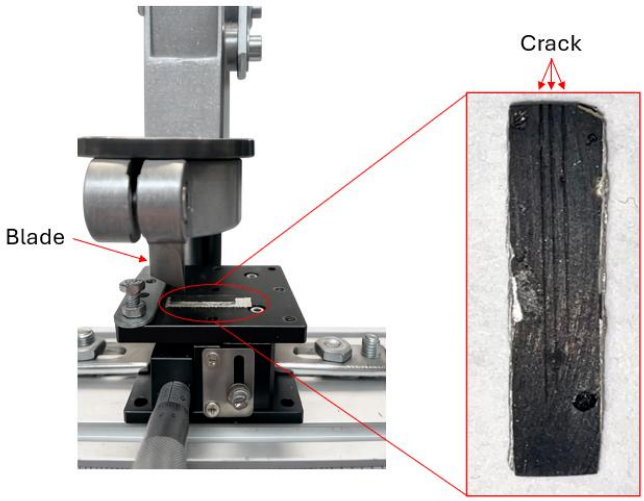

Figure 25 - Micrometer equipment, example of 10 PHR cracks

Prior to the healing treatment, the crack morphology was characterized through 3D topographical measurements performed using a Zeta Instruments Z-20 optical profilometer.

The healing process was subsequently carried out at 180 °C for 5 h 30 min. The healing efficiency (η) was evaluated by comparing two different heating methods: conventional thermal treatment performed in a Carbolite Gero PN30 oven and Joule heating induced using a Keithley Instruments 2410 source meter. During the experiments, the average temperature reached by the specimens was continuously monitored using a FLIR Systems T840 thermal camera.

Finally, the healing efficiency was calculated according to the following equation:

$$\eta\ (\%) = \frac{V_0 - V_f}{V_0} \cdot 100 \qquad (2.12)$$

where V_0 and V_f correspond to the crack volumes measured before and after the healing treatment, respectively.

2.7.6 Micro-tensile measurements

A different experimental approach was adopted to evaluate the healing behaviour of ECO in comparison of the DGEVA system. Due to the consistency limitations of the ECO material, the healing process could not be monitored through crack-topography analysis. Therefore, the healing efficiency was assessed via mechanical characterization using an Hitachi microtensile testing instrument equipped with a 50 N load cell, operating at a

crosshead displacement speed of 1 mm/min. The same specimen geometry employed for DMTA analysis was used for these tests.

The samples were partially overlapped under a constant applied pressure 1.29×10−4MPa to ensure proper interfacial contact and then subjected to two different thermal healing treatments in an oven: the first performed at 70 °C for 30 min, and the second at 120 °C for 6 h. After the healing treatments, tensile measurements were carried out using the same microtensile setup mentioned above in order to evaluate the recovered mechanical strength. The results were finally compared with those obtained from a set of untreated reference specimens.

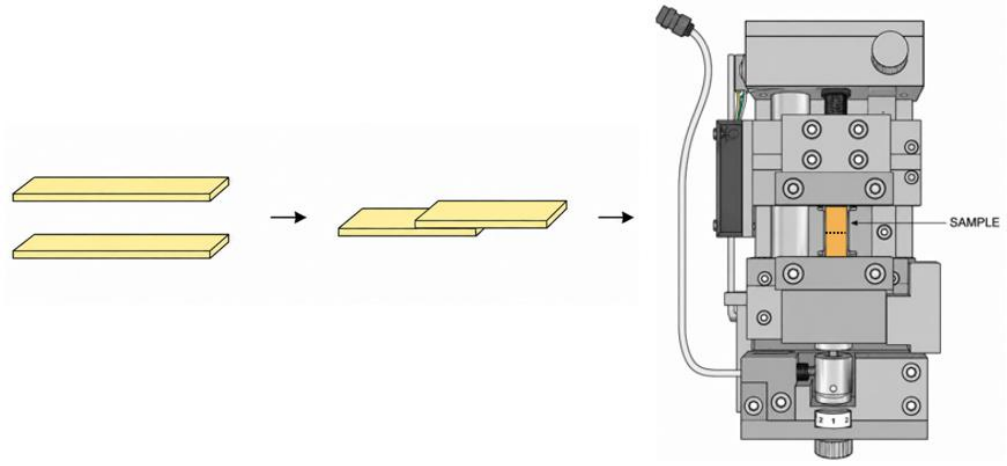

Figure 26 - micro tensile machine setup

3. Results and Discussion

3.1 Liquid Formulation characterization and Curing Behaviour

3.1.1 FT-IR Spectroscopy

For each ECO and DGEVA formulation, the curing process was monitored by Fourier Transform Infrared (FTIR) spectroscopy. Spectra were collected after different exposure times. For the ECO systems, measurements were performed in the DMAX configuration, as described in Section 2.1 (Materials and Methods), at different UV irradiation times (0, 30, 60, 120, 240, 360, 480, 600, and 720 s).

Figure 27 a) shows a representative FTIR spectrum of the pristine ECO formulation and are also indicative of the behaviour observed for the other formulations, which exhibited a similar trend during the curing process. Particular attention was paid to the absorption band at 1727 cm^{-1}, associated with the carboxylic group, which was used as the reference peak, and to the absorption band in the 825–840 cm^{-1} region, corresponding to the oxirane ring.

The intensity of this latter band progressively decreases as the conversion increases, indicating the consumption of epoxy groups during the curing reaction.

Figure 27 b) reports the conversion curves as a function of UV irradiation time for each formulation; the prolonged analysis allowed the determination of the irradiation times required to approach the maximum attainable conversion and to evaluate the evolution of the curing process throughout the entire photopolymerization reaction.

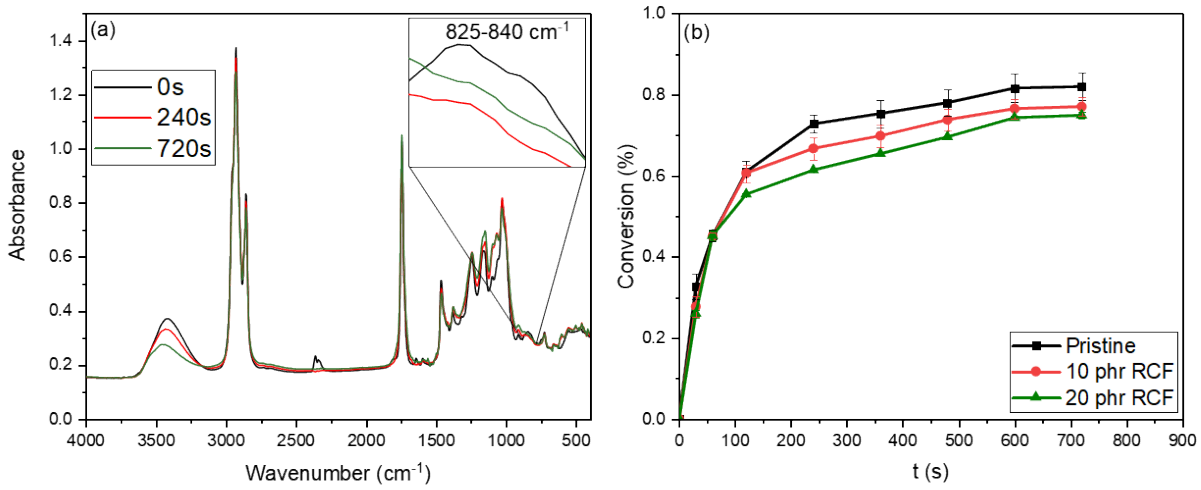

Figure 27 - a) Representative FTIR spectrum of the ECO pristine formulation; Figure 27 b) Conversion curves as a function of irradiation time

This analysis was carried out for all the investigated formulations.

Table 3 reports the conversion values of the three formulations after 720 s of UV irradiation, which were calculated according to the method described in the section above. The results show that the presence of fibers affects the curing process, leading to a partial reduction in the final degree of conversion.

The gel content analysis yielded values higher than 99% for all formulations, confirming the formation of a fully interconnected and insoluble network regardless of filler loading. Notably, the incorporation of 10 and 20 phr of RCF did not produce any statistically significant variation in either the final conversion degree or the gel fraction compared to the pristine resin. This finding demonstrates that the recycled carbon fibers act as inert reinforcing agents and do not interfere with either the stoichiometric balance of the system or the crosslinking efficiency of the epoxy matrix.

RCF content (phr) in ECO matrix	Conversion FTIR [%]	Gel content [%]
0	77 ± 1	99.9 ± 0.1
10	74 ± 1	99.8 ± 0.1
20	61 ± 3	98.2 ± 0.1

Table 3 – ECO FTIR conversion and gel content

Regarding DGEVA, the chemical evolution of the network was investigated by FTIR spectroscopy in transmission mode, following the same experimental approach adopted for

the first matrix system. Figure 28 compares the spectra of the uncured formulation with those collected after the different curing stages, providing insight into the progress of the crosslinking reaction.

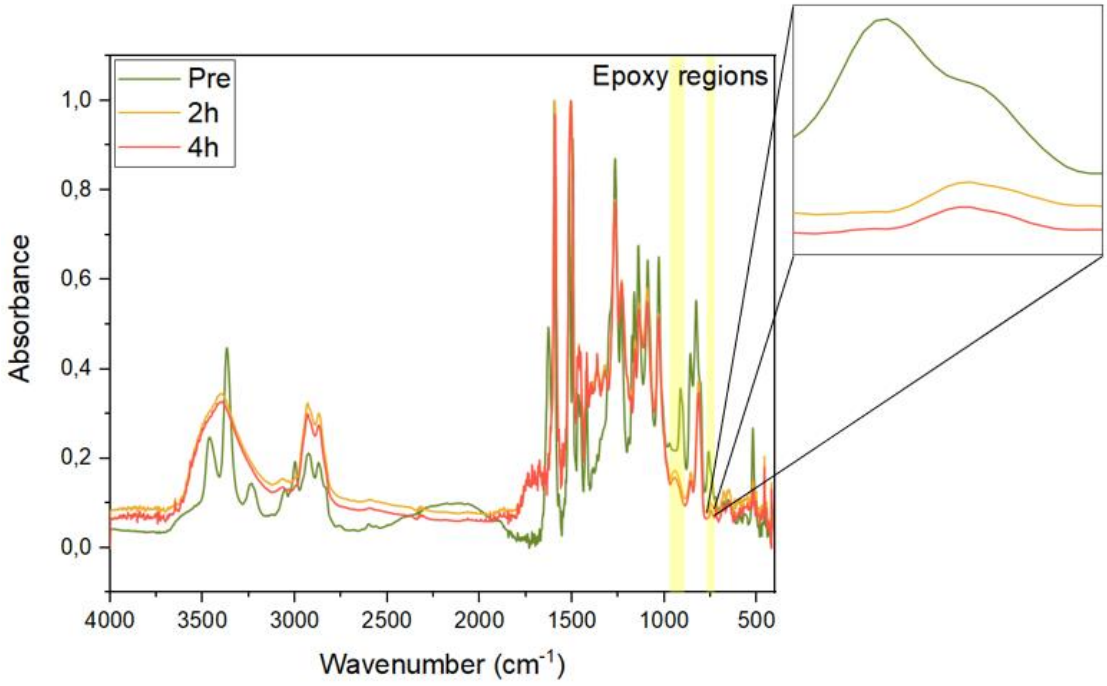

Figure 28 - Representative FTIR spectrum of the DGEVA pristine formulation

As shown, the characteristic absorption bands of the oxirane ring at approximately 915 cm^{-1} and around 770 cm^{-1} progressively decrease in intensity, while a broad hydroxyl stretching band appears in the 3300–3500 cm^{-1} region, confirming the ring-opening polymerization mechanism. To quantify the reaction progress, the epoxide conversion (C) was calculated from the normalized peak areas and plotted as a function of time, as reported in Figure 29.

The kinetic profiles reveal a rapid reaction rate during the first isothermal curing stage (150°C for 1 h). A conversion plateau is reached during the second curing step, as confirmed by extending the curing time up to 4 h, which resulted in negligible spectral variations. This behaviour indicates that the network reaches its topological limit under the applied thermal conditions (150°C for 1 h followed by 200°C for 1 h).

Table 4 summarizes the final conversion values determined by DSC and FTIR, together with the gel content results.

The gel fraction values show a trend consistent with that observed for the overall ECO system.

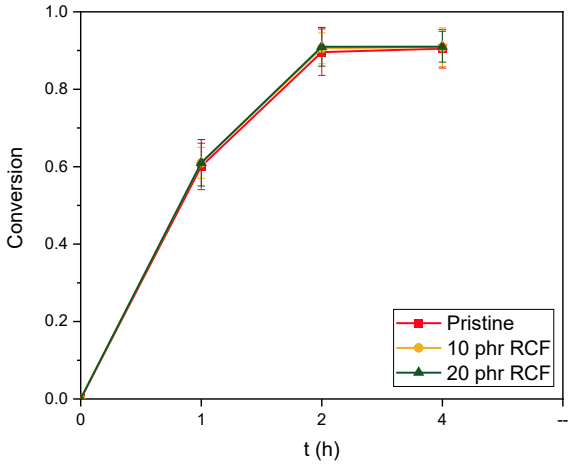

Figure 29 - DGEVA Conversion curves

RCF content (phr) in DGEVA matrix	Conversion FTIR [%]	Gel content [%]
0	91 ± 1	99.9 ± 0.1
10	90 ± 1	99.7 ± 0.1
20	89 ± 1	99.1 ± 0.3

Table 4 - DGEVA FTIR conversion and gel content

3.1.2 Photo-DSC and DSC

For the ECO system, the curing process was investigated by Photo-DSC in order to evaluate the photocuring behaviour and determine the main thermodynamic parameters of the reaction.

As shown in Figure 30 (a) and b)), the Photo-DSC results reveal a progressive decrease in the measured reaction enthalpy with increasing recycled carbon fiber (RCF) content. Specifically, the enthalpy decreases from 175 J g^{-1} for the pristine formulation to 155 J g^{-1} and 115 J g^{-1} for the composites containing 10 phr and 20 phr of RCF, respectively.

This behaviour is consistent with the results obtained from the previous analyses. As the fiber content increases, the curing rate decreases due to the presence of carbon fibers, which partially hinder UV light penetration and absorption within the formulation. Moreover, the filler exerts a physical constraining effect on the developing polymer network, limiting the mobility of the reactive species and consequently reducing the curing efficiency of the matrix.

The conversion values obtained from Photo-DSC and FTIR are in good agreement in terms of their overall trend. In both cases, the degree of conversion decreases as the filler content increases, owing to the same mechanisms discussed above. The slight differences observed in the absolute conversion values can be attributed to the different experimental setups and measurement principles of the two characterization techniques.

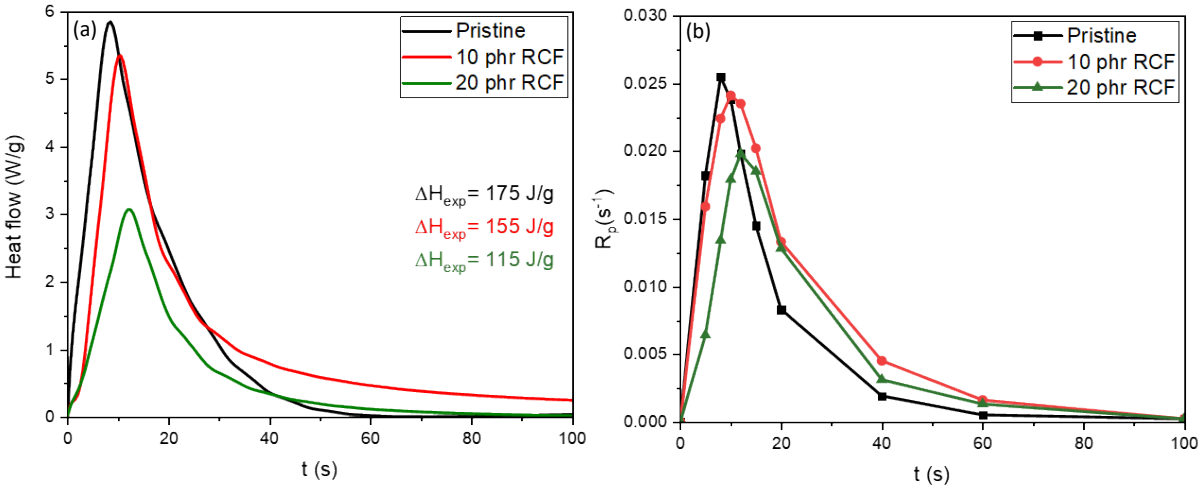

Figure 30 – (a) DSC thermograms of the investigated formulations and (b) Evolution of the polymerization rate as a function of irradiation time

Formulation of ECO matrix	Conversion $_{FTIR}$ (%)	Conversion $_{DSC}$ (%)	Maximum of R_p (s^{-1})
Pristine	82 ± 3	77 ± 1	0.025 ± 0.001
10 phr RCF	77 ± 1	74 ± 1	0.023 ± 0.001
20 phr RCF	74 ± 2	61 ± 3	0.020 ± 0.03

Table 5 - Final conversion values determined by FTIR and Photo-DSC analyses, together with the maximum polymerization rate (Rp,max) for the ECO formulations containing different amounts of RCF

For the DGEVA system, the curing process was investigated through complementary thermal and spectroscopic analyses. In particular, dynamic and isothermal DSC measurements were performed to evaluate the curing behaviour and determine the main thermodynamic parameters of the reaction.

Figure 31 a) shows the dynamic DSC thermograms of the pristine resin and of the formulations containing 10 and 20 phr of recycled carbon fibers (RCF). All samples exhibit a single broad exothermic peak associated with the thermal crosslinking reaction, with an onset temperature (T onset) of approximately 130 °C and an endset temperature (T endset) close to 230 °C. Based on these results, the curing cycle was designed using a first isothermal step at 150 °C for 1 h, aimed at initiating the crosslinking process above T onset, followed by a post-curing stage at 200 °C for 1 h to promote the completion of network formation as the reaction approaches T endset.

The peak temperature (T peak) remains nearly constant at approximately 175 °C for all formulations. Nevertheless, the addition of RCF appears to slightly accelerate the curing process. This behaviour can be attributed to the higher thermal conductivity of carbon fibers, which improves heat transfer throughout the resin and facilitates the curing reaction.

As shown by the isothermal DSC results reported in Figure 31b, the measured reaction enthalpy decreases with increasing fiber content, from 438 J g^{-1} for the pristine formulation to 390 J g^{-1} and 354 J g^{-1} for the composites containing 10 and 20 phr of RCF, respectively. This reduction is mainly related to the dilution effect caused by the presence of the non-reactive filler. However, when the enthalpy values are normalized with respect to the actual resin fraction (w matrix), corrected values of 429 J g^{-1} and 425 J g^{-1} are obtained for the 10

and 20 phr formulations, respectively. These values are very close to that of the pristine resin, indicating that the incorporation of RCF does not significantly hinder the curing reaction nor adversely affect the final degree of conversion of the polymer network.

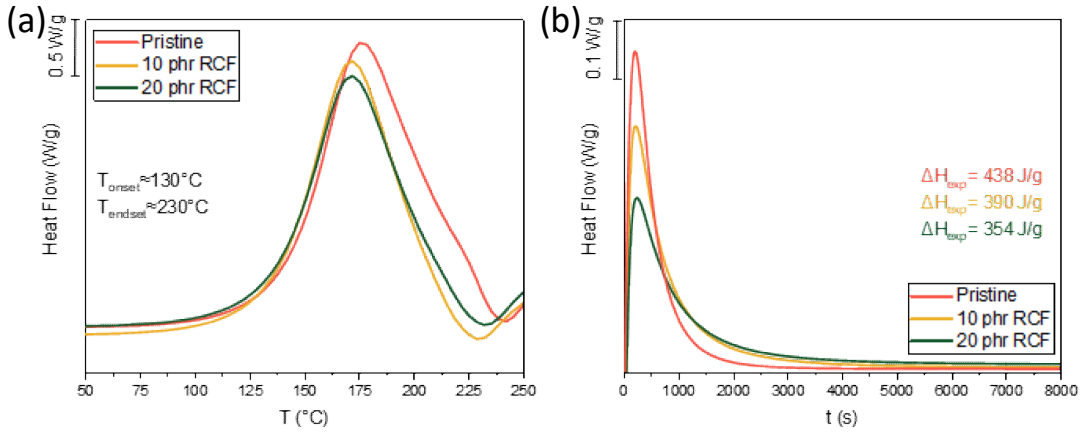

Figure 31 - Dynamic (a) and isothermal (b) DSC graphs for all the studied formulations

Table 6 summarizes the final conversion values obtained by DSC and FTIR, together with the corresponding gel content. A discrepancy is observed between the DSC conversion (CDSC ≈ 76–79%) and the FTIR conversion (CFTIR ≈ 89–91%, calculated from the peak at 770 cm^{-1}). This difference is commonly observed in highly crosslinked epoxy systems and can be attributed to vitrification effects and restricted molecular mobility during the final stages of curing, which reduce the residual heat detected by DSC while FTIR continues to monitor the consumption of reactive groups. (50).

Formulation of DGEVA matrix	Conversion $_{FTIR}$ (%)	Conversion $_{DSC}$ (%)	ΔH_{exp} [J/g]
Pristine	91±1	79±2	438 ±2
10 phr RCF	90±1	77±2	390 ±4
20 phr RCF	89±1	76±2	354 ±4

Table 6 - Summary of the final degree of conversion values determined by FTIR and Photo-DSC analyses for the investigated DGEVA formulations

3.1.3 Rheology

Rheological measurements were carried out on both formulations, under identical mixing conditions, in order to assess the variation in viscosity as a function of the previously described carbon fibre filler content. This aspect is particularly relevant for understanding how the fibres can disperse within the matrix depending on its viscosity. For both systems,

the same general trend was observed. In the case of the ECO formulation, the viscosity increased with increasing filler concentration, as illustrated in Figure 32.

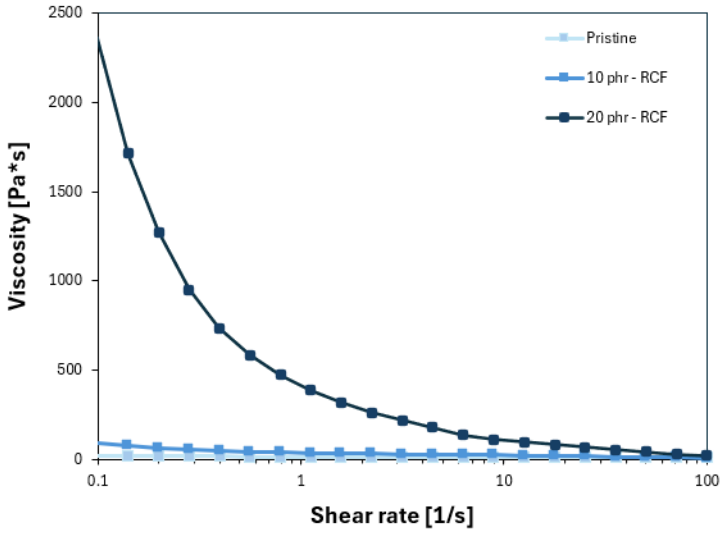

Figure 32 - rheometry of ECO system

Subsequently, the same analysis was also performed on the DGEVA formulation, where the same trend was observed. In particular, starting from the pristine system and then increasing the carbon fibre content to 10 phr and subsequently to 20 phr, the viscosity progressively increased, as shown in Figure 33.

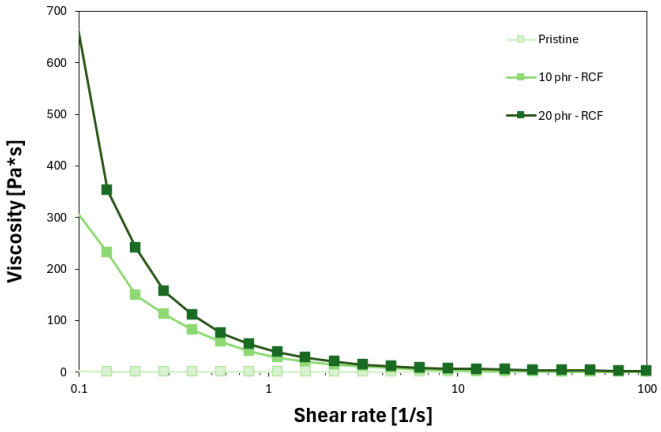

Figure 33 rheometry of DGEVA system

In this context, a rheological comparison was performed among the pristine, 10 phr, and 20 phr formulations in order to investigate how the same recycled fibres can be dispersed differently depending on the type of matrix. The rheological tests were carried out at the respective mixing temperatures. For the ECO formulation, measurements were performed at room temperature (25 °C), whereas for the DGEVA system, which tends to crystallize at room temperature, the material was first heated to 80 °C in an oven and manually pre-mixed prior to the mixing process. Consequently, rheological measurements were

conducted at an intermediate temperature of approximately 45 °C to prevent crystallization during testing.

Subsequently, a figure is presented illustrating the comparison between the pristine, 10 phr, and 20 phr systems for the two different matrices investigated.

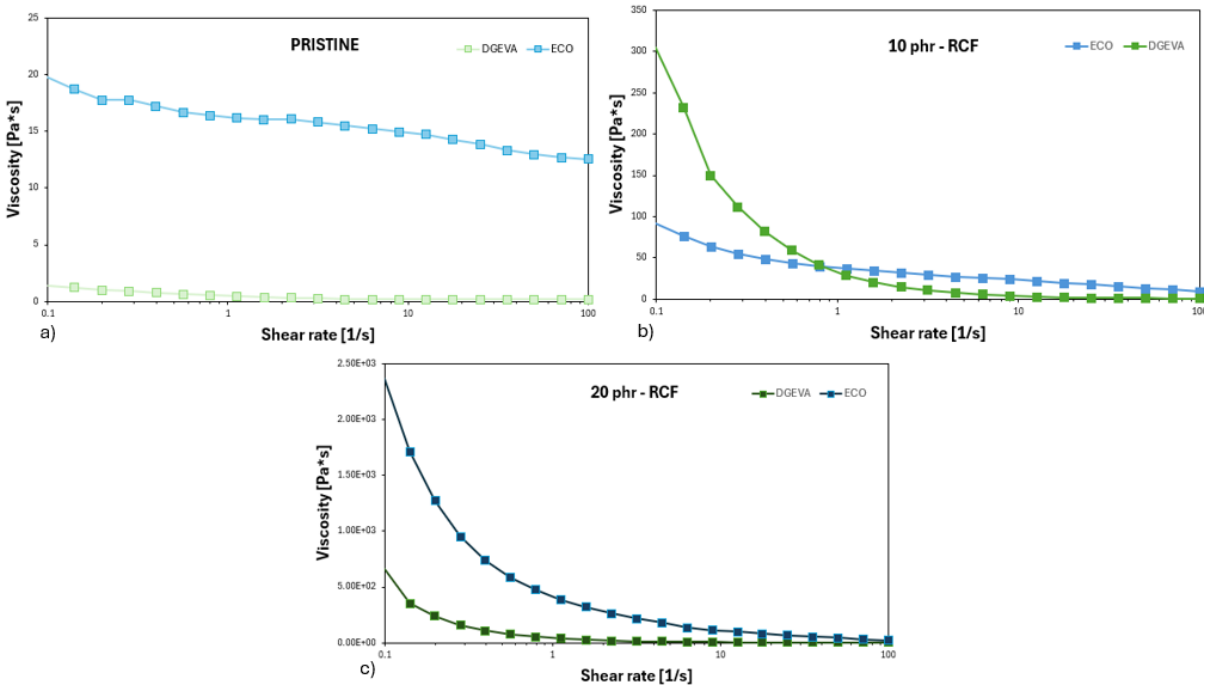

*Figure 34 - Viscosity versus shear rate curves for DGEVA- and ECO-based formulations containing **(a)** 0 phr (pristine), **(b)** 10 phr, and **(c)** 20 phr of recycled carbon fibers (RCF), illustrating the effect of fiber loading and matrix type on the rheological response.*

As can be observed across the entire range within the operating window of the Thinky mixer used for fibre dispersion, the DGEVA formulation consistently exhibits a lower viscosity. This behaviour may partially explain why the fibres appear to be more uniformly and effectively dispersed in the DGEVA system compared to the ECO formulation, where the higher viscosity could limit fibre mobility and hinder an optimal distribution within the matrix (30).

3.1.4 Microstructural analysis

SEM observations were carried out only on the ECO-based composites. The micrographs were acquired on brittle fracture surfaces obtained by immersing the specimens in liquid nitrogen prior to fracture, in order to evaluate the dispersion of the recycled carbon fibers (RCFs) within the polymer matrix and to investigate the fiber–matrix interfacial interaction.

The SEM images shown in Figure 35(a–c) provide information on the fracture morphology of the composites. In particular, Figure 35(a) highlights the good interfacial adhesion between the ECO matrix and the recycled carbon fibers, as evidenced by fibers fractured

close to the matrix surface rather than being completely extracted, suggesting efficient stress transfer across the interface. Conversely, Figure 35(b) shows evidence of the fiber pull-out mechanism, indicating that debonding between the fiber and the matrix also contributes to the fracture process.

Figure 35(c) corresponds to the fracture surface of the ECO composite containing 10 phr of recycled carbon fibers and reveals a compact and well-polymerized morphology, with a relatively homogeneous distribution of the reinforcement.

The FESEM image in Figure 35(d) corresponds to the ECO composite containing 20 phr of recycled carbon fibers. Compared with the 10 phr formulation, the fracture surface exhibits the presence of several internal voids and defects, which are likely associated with the higher fiber loading.

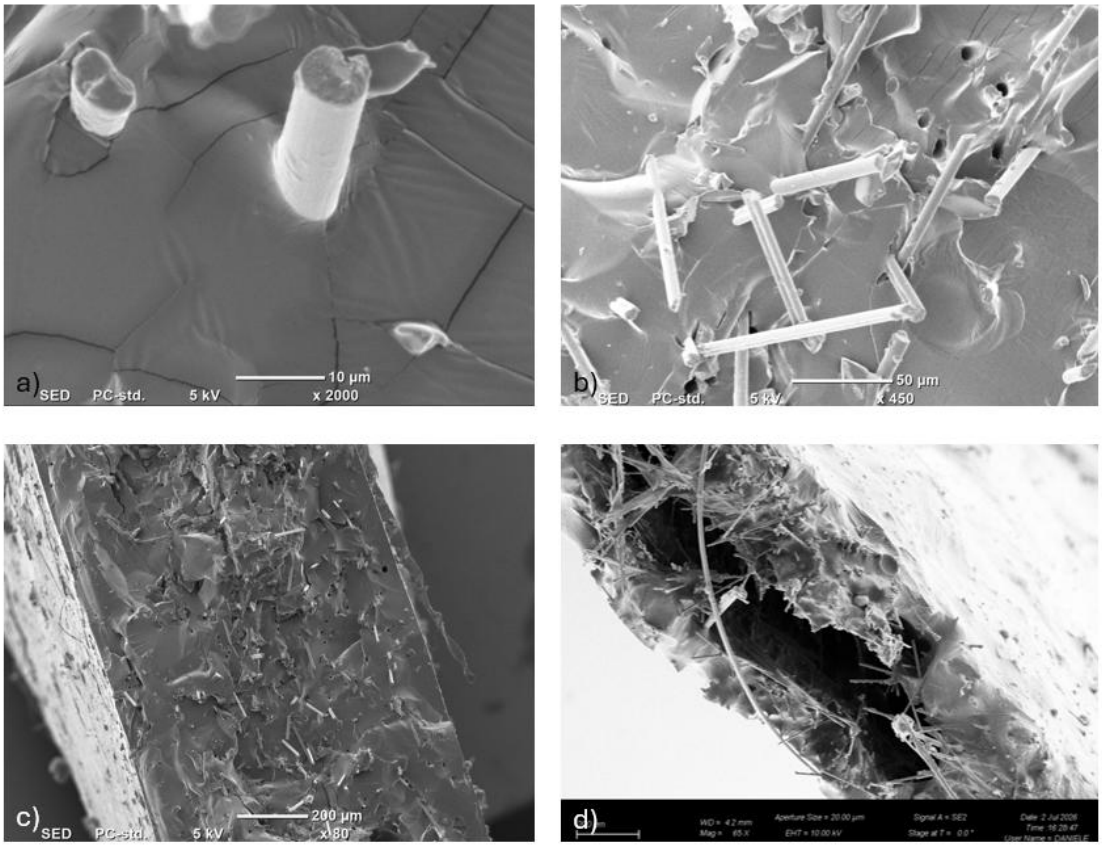

Figure 35 – SEM images of ECO composites reinforced with recycled carbon fibers (RCFs): (a) good interfacial adhesion between the ECO matrix and the carbon fibers; (b) fiber pull-out mechanism observed on the fracture surface; (c) dispersion of 10 phr recycled carbon fibers within the ECO matrix. (d) FESEM image showing the dispersion of 20 phr recycled carbon fibers within the ECO matrix.

3.1.5 Contact Angle

Contact angle measurement is necessary because the main application of the materials is as coatings, for which wettability is a key parameter to consider. In particular, evaluating the hydrophilic or hydrophobic behaviour of the surface is essential. Hydrophilicity and hydrophobicity strongly influence the final performance of the coating. For example, wettability can affect properties such as adhesion, moisture resistance, durability, and surface fouling behavior. Therefore, contact angle analysis provides a useful way to correlate surface characteristics with the functional properties of the coating.

Table 7 reports the water contact angle values measured for the different composite formulations. For both resin systems, the same trend was observed: the contact angle increased with increasing recycled carbon fiber (RCF) content. This behaviour can be attributed to the lower wettability of carbon fibers compared to the polymer matrices. As the fiber content increases, a larger fraction of the composite surface is occupied by carbon fibers, leading to a reduction in the overall surface wettability and, consequently, to higher contact angle values.

A comparison between the two matrices reveals that the ECO-based formulations exhibited consistently lower contact angles than the DGEVA-based systems. This result indicates a higher surface wettability of ECO, which can be attributed to the presence of more polar functional groups within its chemical structure. In particular, ECO contains hydroxyl (-OH) and ester (-COO-) groups that enhance the interaction with water molecules. In contrast, the DGEVA network contains fewer accessible polar functionalities and a higher proportion of aromatic structures, resulting in a lower surface polarity and therefore higher contact angle values.

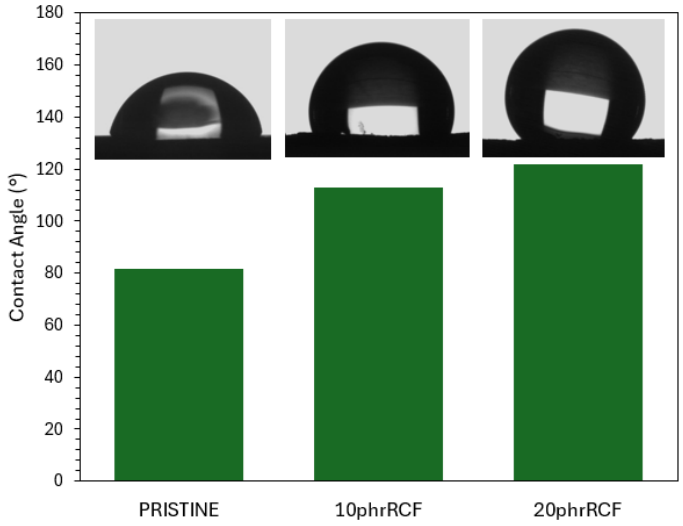

Figure 37 - DGEVA contact angles

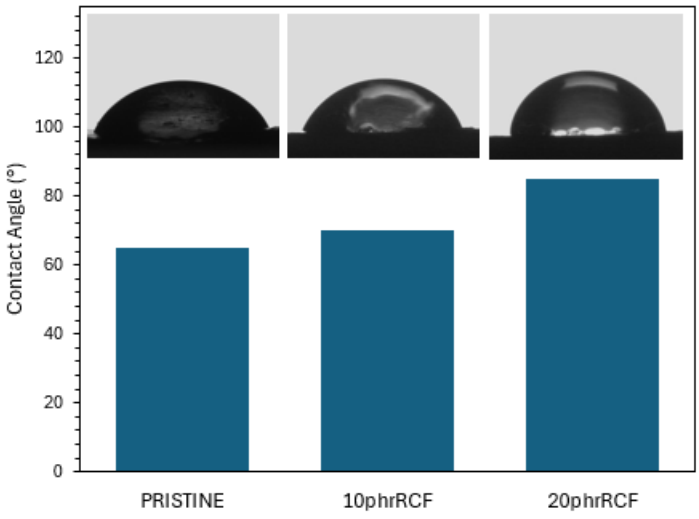

Figure 36 - ECO contact angles

RCF content (phr)	Contact angle (°) ECO	Contact angle (°) DGEVA
0	65 ± 3	82 ± 2
10	70 ± 3	113 ± 3
20	85 ± 5	122 ± 3

Table 7 - contact angle values

3.2 Thermomechanical and mechanical properties of crosslinked coatings

3.2.1 DMTA

The thermal and viscoelastic properties of the ECO formulations were evaluated by DSC and DMTA analyses. Figures 38 (a) and 38 (b) report the DSC thermograms and the temperature dependence of the loss factor (Tanδ), respectively.

For the pristine formulation, the glass transition temperature (Tg) was determined to be approximately −18 °C from DSC measurements and 2 °C from the maximum of the Tanδ peak. The incorporation of recycled carbon fibers (RCF) did not produce a significant variation in Tg. Indeed, the DSC thermograms show Tg values of about −18 °C, −18 °C, and −17 °C for the pristine, 10 phr RCF, and 20 phr RCF formulations, respectively. Similarly, DMTA analysis revealed Tg values of 2 °C, 0 °C, and 2 °C, indicating only minor fluctuations within the experimental uncertainty.

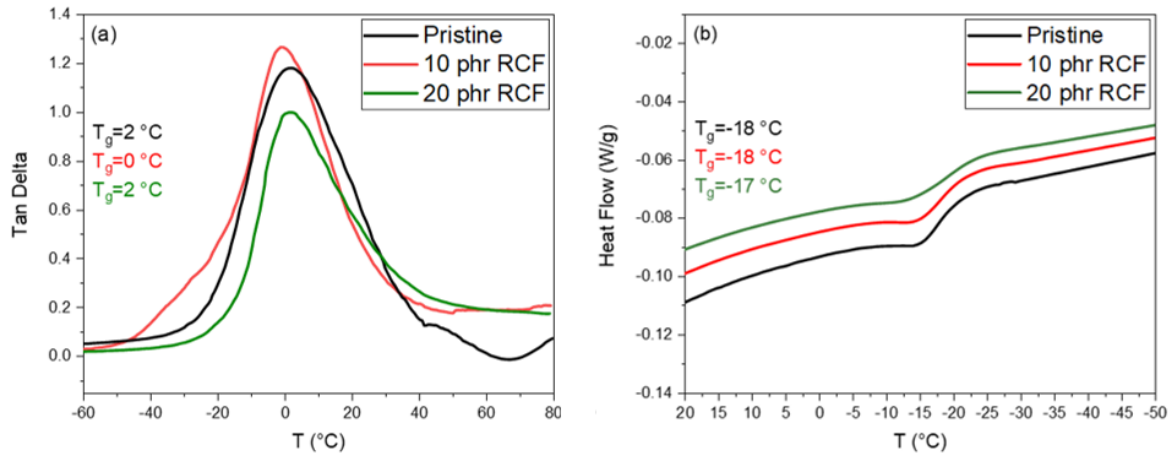

Figure 38 - (a) DSC thermograms of the pristine ECO resin and RCF-reinforced formulations used to determine the glass transition temperature (Tg) - (b) Tanδ curves as a function of temperature for the investigated ECO formulations

Figure 39 shows the evolution of the storage modulus (E') as a function of temperature. Although the addition of RCF does not significantly affect Tg, it markedly increases the modulus in the rubbery region. The E' value at Tg + 50 °C rises from 0.06 MPa for the pristine resin to 2.4 MPa and 2.6 MPa for the 10 and 20 phr composites, respectively, demonstrating the reinforcing effect of recycled carbon fibers and the improved thermomechanical stability of the resulting networks.

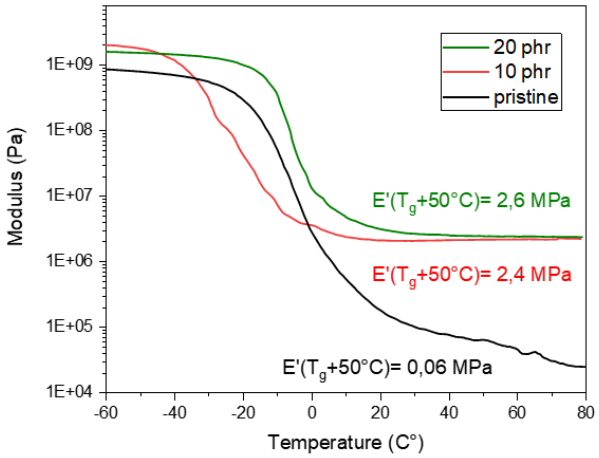

Figure 39 - Storage modulus (E') as a function of temperature for the pristine ECO formulation and the composites containing 10 and 20 phr of recycled carbon fibers (RCF)

Formulation	$T_{g,\ DMTA}$ (°C)	$T_{g,\ DSC}$ (°C)	ν_c (mol/m³)
Pristine	2±1	-18±1	7±1
10 phr RCF	0±1	-18±3	298±9
20 phr RCF	2±1	-17±2	320±12

Table 8 - Glass transition temperatures determined by DMTA and DSC, together with the corresponding crosslink density (v)

For the DGEVA system the thermal and viscoelastic behavior of the cured formulations was investigated by DSC and DMTA analyses. The DSC thermograms and the temperature dependence of the loss factor (Tanδ) are reported in Figures 40(a) and 40(b), respectively. For the pristine resin, the glass transition temperature (Tg) was determined to be 121 °C by DSC and 122 °C from the maximum of the Tanδ peak. The incorporation of recycled carbon fibers (RCF) resulted in a gradual increase in Tg, as evidenced by both characterization techniques. In particular, DSC measurements revealed Tg values of 123 °C and 127 °C for the formulations containing 10 and 20 phr of RCF, respectively, while DMTA showed a shift of the Tanδ maximum to approximately 126 °C for the reinforced systems.

The increase in Tg can be attributed to the rigid nature and high aspect ratio of the carbon fibers, which restrict the mobility of the polymer chains at the fiber–matrix interface and hinder cooperative segmental motions. In addition, increasing the RCF content leads to a marked reduction in the intensity of the Tanδ peak. This decrease in damping behavior is associated with both the replacement of part of the viscoelastic polymer phase by the rigid filler and the formation of an immobilized polymer layer surrounding the fiber surface. The reduced area under the Tanδ curve further indicates a transition toward a more elastic response dominated by energy storage rather than energy dissipation.

The reinforcing effect of RCF is also reflected in the storage modulus measured within the rubbery plateau region (T > Tg + 50 °C), as shown in Figure 41 and summarized in Table 9. The storage modulus increases significantly from approximately 2 MPa for the pristine

network to 10 MPa and 55 MPa for the formulations containing 10 and 20 phr of RCF, respectively. To further evaluate this behaviour, the effective crosslink density (νc) was calculated. The apparent νc values increased from 198 mol m^{-3} for the neat resin to 875 mol m^{-3} and 4918 mol m^{-3} for the 10 and 20 phr composites, respectively.

It is important to emphasize that this substantial increase in νc does not correspond to an actual change in the chemical crosslinking density of the network. Indeed, DSC and FTIR analyses (Table 4) confirmed a comparable degree of conversion for all formulations. Therefore, the increase in the calculated νc should be interpreted as an apparent effect arising from physical reinforcement. The rigid carbon fiber network contributes to stress transfer in the rubbery state, while the immobilized polymer chains at the fiber–matrix interface act as additional physical constraints. These results demonstrate that RCFs provide significant reinforcement at elevated temperatures without affecting the curing efficiency or the chemical structure of the epoxy network.

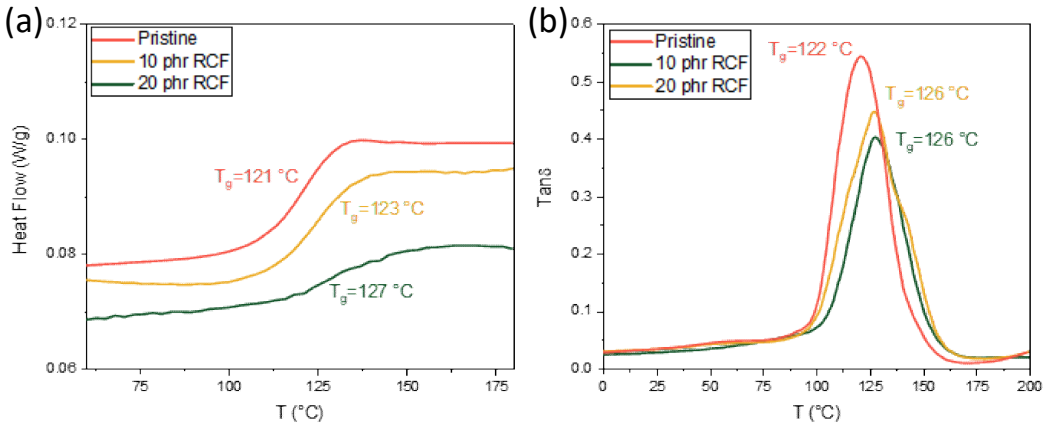

Figure 40 - (a) DSC thermograms and (b) Tanδ curves obtained by DMTA for the pristine DGEVA resin and the formulations containing 10 and 20 phr of recycled carbon fibers (RCF). The glass transition temperatures (Tg) determined by each technique are indicated

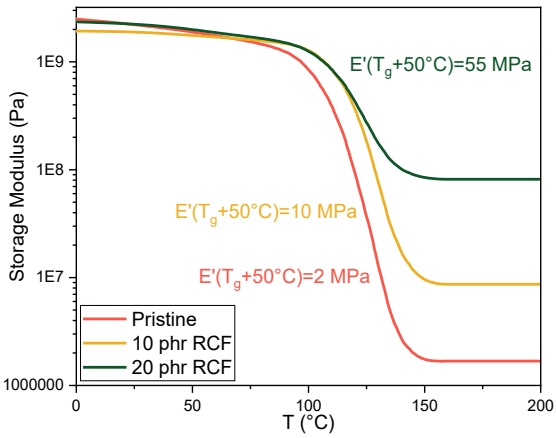

Figure 41 - DMTA storage modulus (E') curves of pristine and RCF-reinforced DGEVA formulations.

Formulation	$T_{g,\,DMTA}$ (°C)	$T_{g,\,DSC}$ (°C)	$E'(Tg + 50°C)$ [MPa]	v_c (mol/m³)
Pristine	122±1	121±2	2.2±0.5	180±45
10 phr RCF	126±1	123±4	9.8±1.1	893±98
20 phr RCF	126±1	127±1	55.1±2.0	4909±178

Table 9 - Thermomechanical properties and crosslink density of pristine and RCF-reinforced DGEVA formulations.

3.2.2 TGA

Thermogravimetric analysis (TGA) was performed on the cured formulations of both matrices to evaluate their thermal stability. This assessment is particularly important for defining the temperature limits during the healing process, ensuring that the material is not exposed to temperatures that could induce thermal degradation either during healing or under potential service conditions.

The temperature corresponding to 5% weight loss, denoted as T(5%), is commonly considered the onset degradation temperature. It represents the temperature at which the sample begins to undergo significant thermal decomposition, as identified by a mass loss of 5%.

For both formulations, thermogravimetric (TG) and derivative thermogravimetric (DTG) curves were obtained under a dry air atmosphere.

Starting with the ECO system, the 20 phr formulation was analyzed and the corresponding TG and DTG curves are reported in Figure 42. The onset degradation temperature, identified by T(5%), was found to be approximately 220°C, while the maximum degradation rate, corresponding to the DTG peak (Tmax), occurred at 323°C. Based on these results, particular attention was paid during all subsequent manufacturing and healing procedures, whether performed in a conventional oven or through Joule heating, to ensure that the operating temperature remained below the onset degradation temperature T(5%), thus preventing any thermally induced damage to the material.

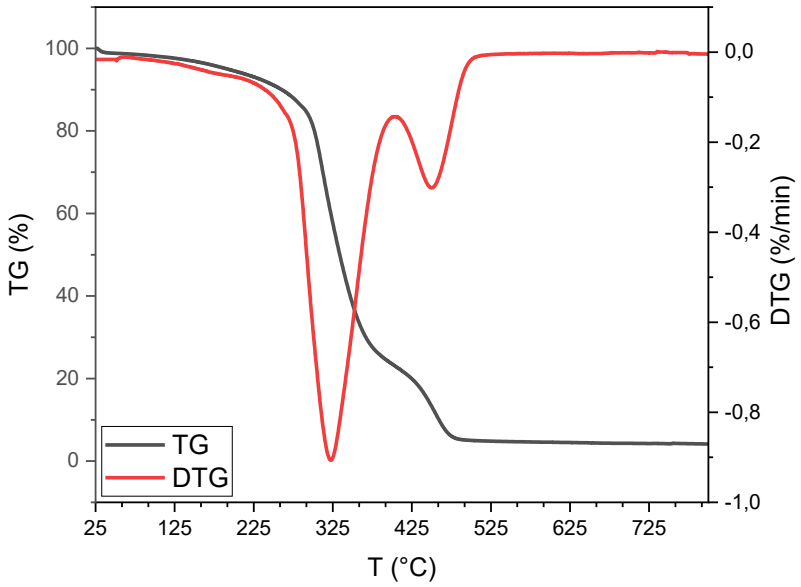

Figure 42 - G and DTG thermograms of the cured resin under the selected heating conditions.

Moving to the DGEVA system, the thermal stability of both the pristine formulation and the composite reinforced with 20 phr of recycled carbon fibers (RCF) was investigated in order to evaluate the effect of the filler on the thermal behavior of the matrix. The TG and DTG curves are presented in Figure 43 (a) and (b), respectively. The incorporation of 20 phr of RCF resulted in a substantial improvement in thermal stability. The degradation onset temperature, T(5%), increased from approximately 250°C for the pristine matrix to 350°C for the composite. Similarly, the maximum degradation temperature (Tmax), identified from the minimum of the DTG curve, shifted from approximately 330°C to 410°C.

This remarkable enhancement can be attributed to the intrinsically high thermal stability of carbon fibers and to their role as a physical mass-transport barrier (tortuous path effect), which hinders the diffusion of volatile degradation products from the bulk material to the surrounding atmosphere. Furthermore, the residual mass measured at 900°C is consistent with the expected fiber content, confirming the excellent thermal resistance of the recycled carbon fibers. In contrast, the negligible residue observed for the pristine matrix indicates the almost complete volatilization of the polymeric phase during thermal degradation.

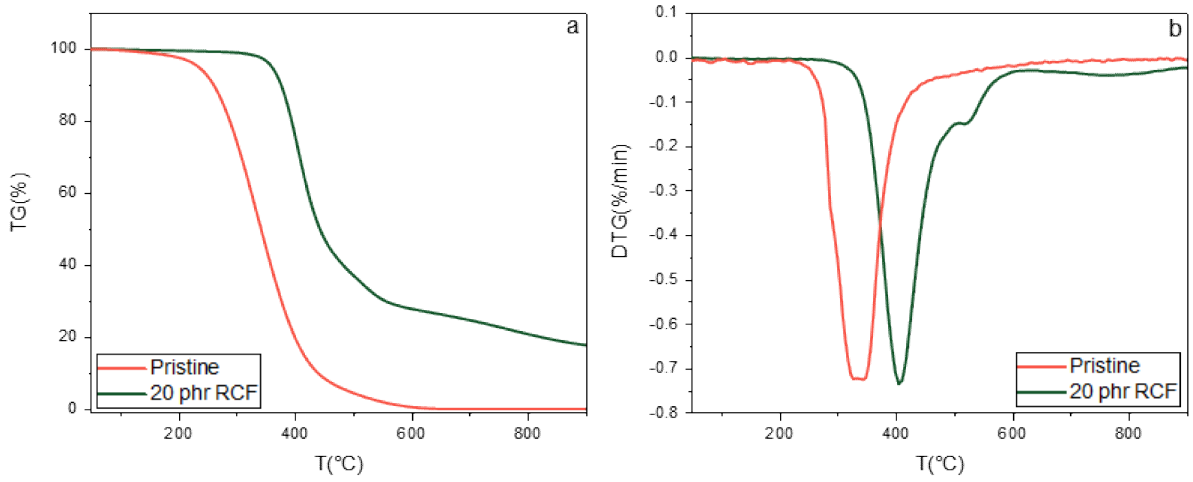

Figure 43 - TG thermograms and DTG thermograms of the pristine resin and the 20 phr RCF composite.

3.2.3 Tensile Test

Starting with ECO tensile tests were performed to assess the mechanical properties of the materials as described in Section 2.7.2. The Young's modulus, rupture stress, and rupture strain were determined from the corresponding stress–strain curves for each matrix formulation and carbon fiber loading. The graph 44 shown presents the average stress–strain response obtained from three specimens tested for each of the three formulations.

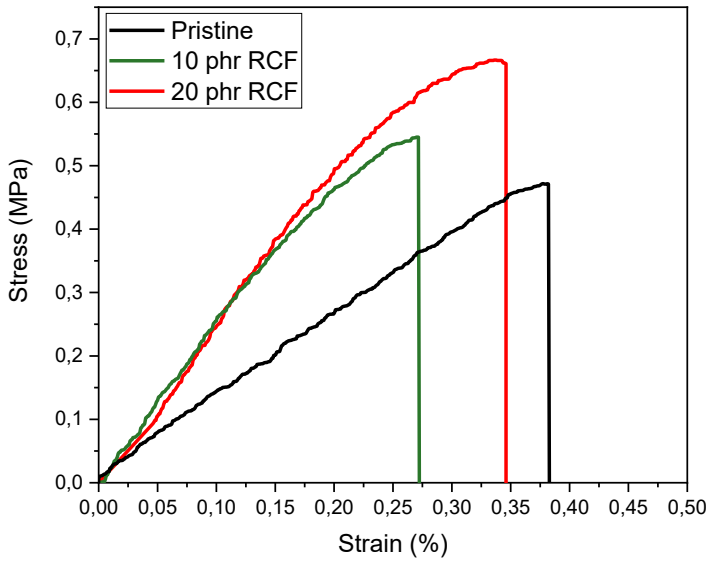

Figure 44 - Stress–strain curves obtained from tensile tests for the pristine resin and the RCF-reinforced formulations of ECO system

As can be observed, increasing the fiber content leads to a steeper stress–strain curve, indicating an increase in material stiffness. In particular, the specimen containing 20 phr of

fibers reaches higher rupture stress and rupture strain values than the 10 phr specimen, highlighting an overall improvement in mechanical performance.

RCF content (phr) of ECO system	E [MPa]	Rupture stress [MPa]	Rupture strain [%]
0	1.2	0,47	0,38
10	2.4	0,54	0,27
20	2.6	0,66	0,35

Table 10 - Tensile properties of the ECO formulations as a function of recycled carbon fiber (RCF) content, including Young's modulus (E), rupture stress, and rupture strain.

As can be observed both qualitatively from the graph and quantitatively from the values reported in the table, the addition of RCF leads to a progressive increase in both Young's modulus and rupture stress. In contrast, the specimen containing 10 phr RCF exhibits a lower rupture strain, indicating a reduced ability to deform before failure.

Moving to DGEVA, Figure 45 and Table 11 show that the addition of RCF progressively increases the Young's modulus and, at 20 phr, significantly improves both the tensile strength and the strain at break. While the 10 phr composite does not exhibit a substantial increase in strength and shows a slight reduction in elongation at break, the 20 phr formulation displays a pronounced reinforcing effect. This behavior can be attributed to the formation of a fiber network that promotes efficient load transfer and hinders crack propagation, resulting in enhanced stiffness, strength, and ductility.

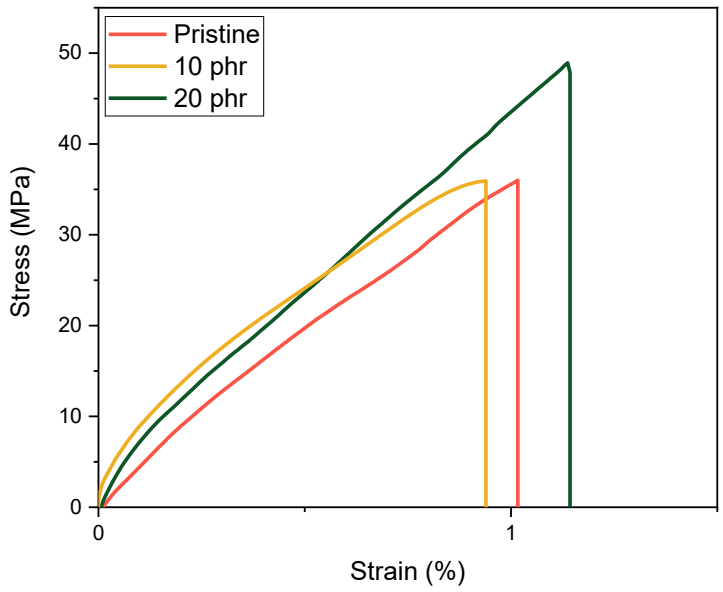

Figure 45 - Stress–strain curves obtained from tensile tests for the pristine resin and the RCF-reinforced formulations of DGEVA system

RCF content (phr) of DGEVA system	E [GPa]	Rupture stress [MPa]	Rupture strain [%]
0	3.6 ± 0.2	36 ± 2	1.0 ± 0.1
10	4.2 ± 0.3	36 ± 2	0.9 ± 0.1
20	4.6 ± 0.4	51 ± 2	1.2 ± 0.1

Table 11 - Tensile properties of the ECO formulations as a function of recycled carbon fiber (RCF) content, including Young's modulus (E), rupture stress, and rupture strain

A brief comparison between the two matrices shows that, despite the addition of the same amount of reinforcing agent, the mechanical properties differ significantly. The Young's modulus is three orders of magnitude higher in DGEVA than in ECO. This was already expected from the glass transition temperature (Tg) analysis, which indicates that in the case of ECO the Tg is below room temperature.

3.3 Thermo-electrical measurements

The first measurement carried out was the electrical conductivity, which was evaluated using Ohm's law (3.1). The slope of the I–V curve was used to determine the resistance, and the resistivity was then calculated according to Equation (3.2). Finally, the conductivity was obtained as the inverse of the resistivity (3.3).

$$R = \frac{V}{I} \qquad \rho = \frac{R * A}{L} \qquad \sigma = \frac{1}{\rho} \qquad (3.1)\ (3.2)\ (3.3)$$

Where R is the resistance (Ω), V the voltage (V), I the current (A), ρ the resistivity (Ω·m), A the cross-sectional area (m^2), L the length (m), and σ the electrical conductivity (S/m).

Starting from DGEVA, three samples containing 10 phr RCF and four samples containing 20 phr RCF were analyzed. The pristine formulation could not be measured using the equipment described in Section 2.7.1; however, it is well established that electrically insulating polymers typically exhibit conductivities on the order of 10^{-11} S/m.

Figure 46 and Table 12 show the electrical conductivity of the developed composites. As expected for DGEVA, the conductivity increases as the RCF content increases. This behaviour is related to the formation of a greater number of conductive pathways inside the material.

The electrical percolation threshold is estimated to be around 10 phr for this system.

The composites reinforced with 20 phr of RCF show relatively high conductivity values, which are consistent with those reported in the literature for similar systems.

RCF content (phr)	Electrical conductivity (S/m)	Stdev
0	1.00E-11	0
10	4.59E-03	4.55E-03
20	2.05E+01	1.08E+01

Table 12 -DGEVA Electrical conductivity as a function of RCF content

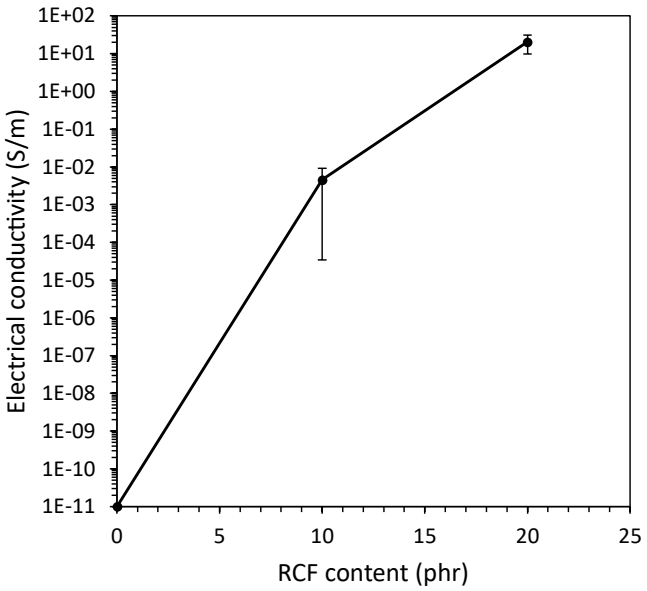

Figure 46 - DGEVA Electrical conductivity as a function of RCF content

Moving on to the Joule heating characterization, the temperature increase is described by Equation (3.4). As shown, the temperature rises with increasing current and applied voltage.

$$Q = I \cdot V \cdot t \tag{3.4}$$

where Q is the heat generated by the Joule effect, I is the current intensity, V is the applied voltage, and t is the time.

Regarding the electrical conductivity of ECO, three samples with 20 phr and three samples with 10 phr were analysed. However, the results did not follow the same trend observed for the DGEVA matrix. In this case, the increase in recycled carbon fiber content was not consistent with Equation (3.4), likely due to the presence of voids within the 20 phr ECO matrix caused by the higher fiber loading. As a result, the 10 phr samples showed higher conductivity values than both the pristine and 20 phr samples.

Table 13 reports the average electrical conductivity values.

RCF content (phr)	Electrical conductivity (S/m)	Stdev
0	1.00E-11	0
10	3.57E-03	9.89E-05
20	5.07E-04	4.24E-04

Table 13 - ECO Electrical conductivity as a function of RCF content

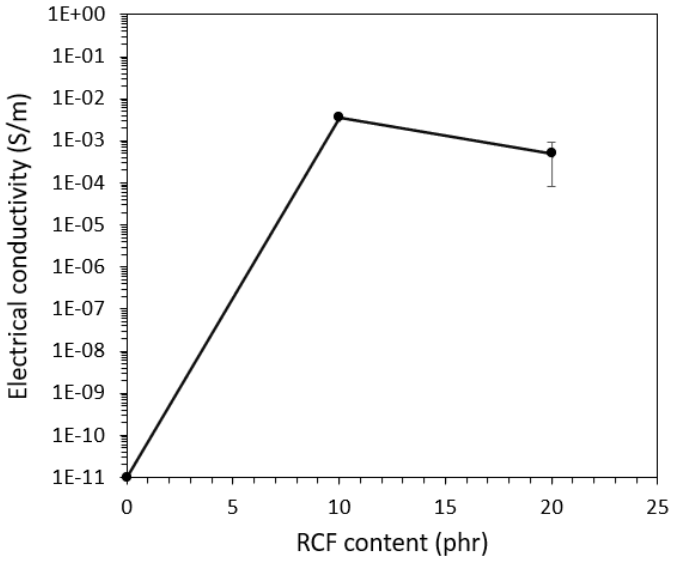

Figure 47 - ECO Electrical conductivity as a function of RCF content

Following the electrical conductivity analysis, the Joule heating behavior of both matrices was investigated using the experimental setup described in Section 2.7.1. Specifically, the applied voltage was supplied through a Keithley 2410 SourceMeter, while the temperature distribution was monitored using a FLIR T840 thermal imaging camera.

For the DGEVA matrix, the results were consistent with those obtained from the electrical conductivity measurements. An increase in the RCF content led to a significant enhancement of the Joule heating performance, enabling comparable target temperatures to be achieved at substantially lower applied voltages.

For example, to reach an average temperature of approximately 100 °C, composites containing 10 phr of RCF required an applied voltage of 60 V, whereas a voltage lower than 2.5 V was sufficient for composites containing 20 phr of RCF. This behaviour can be attributed to the increase in the electrical conductivity of the material. As conductivity increases, higher currents can flow under a given applied voltage, resulting in greater power dissipation and, consequently, higher heat generation through the Joule effect.

Figures 48 (a) and 48 (b) illustrate the difference in the voltages required to achieve the same target temperature for composites with different RCF contents. Furthermore, a substantial difference between the average temperature and the maximum temperature can be observed for the two RCF loadings, highlighting the influence of filler concentration not only on the heating efficiency but also on the uniformity of the temperature distribution within the composite, that follow Formula 3.5.

$$joule\ heating\ homogeneity\ = \frac{1 - (T_{max} - T_{avarage})}{T_{max}} \tag{3.5}$$

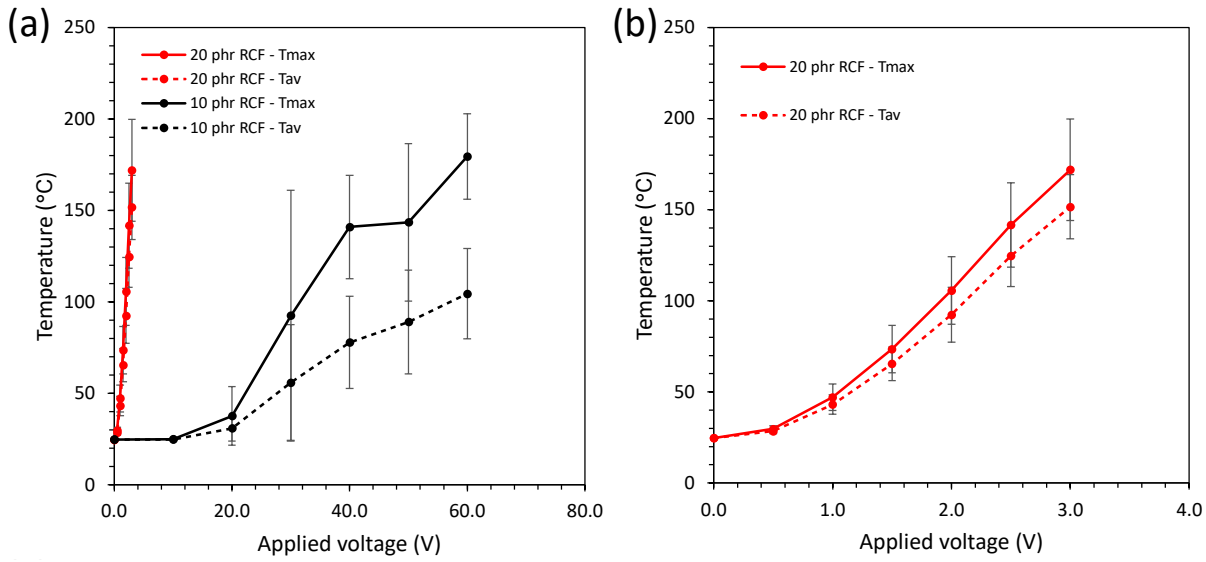

Figure 48 - Average and maximum temperatures reached by joule heating in DGEVA

As described in Section 2.7.1, a thermographic image was acquired after each voltage increment in order to monitor the temperature distribution across the specimens during Joule heating. The thermograms reported in Figure 49 (a) and (b) allow for the evaluation of the heating homogeneity within the composites.

The specimens reinforced with 20 phr of RCF exhibited a more uniform temperature distribution compared to those containing 10 phr of RCF. The lower heating homogeneity observed in the latter can be attributed to their significantly lower electrical conductivity, as this formulation is close to the electrical percolation threshold. Under these conditions, the conductive network is not fully developed, and the electrical current tends to flow preferentially through a limited number of conductive pathways. As a result, localized regions of higher current density are generated, leading to the formation of hot spots and a less uniform temperature distribution.

Conversely, at RCF contents well above the percolation threshold, the conductive network becomes increasingly interconnected and dense, providing multiple parallel pathways for charge transport. This facilitates a more uniform distribution of the electrical current throughout the material, thereby promoting more homogeneous heat generation by the Joule effect and reducing temperature gradients across the specimen. Consequently,

composites containing 20 phr of RCF exhibit superior heating uniformity and improved thermal distribution compared to those reinforced with 10 phr of RCF.

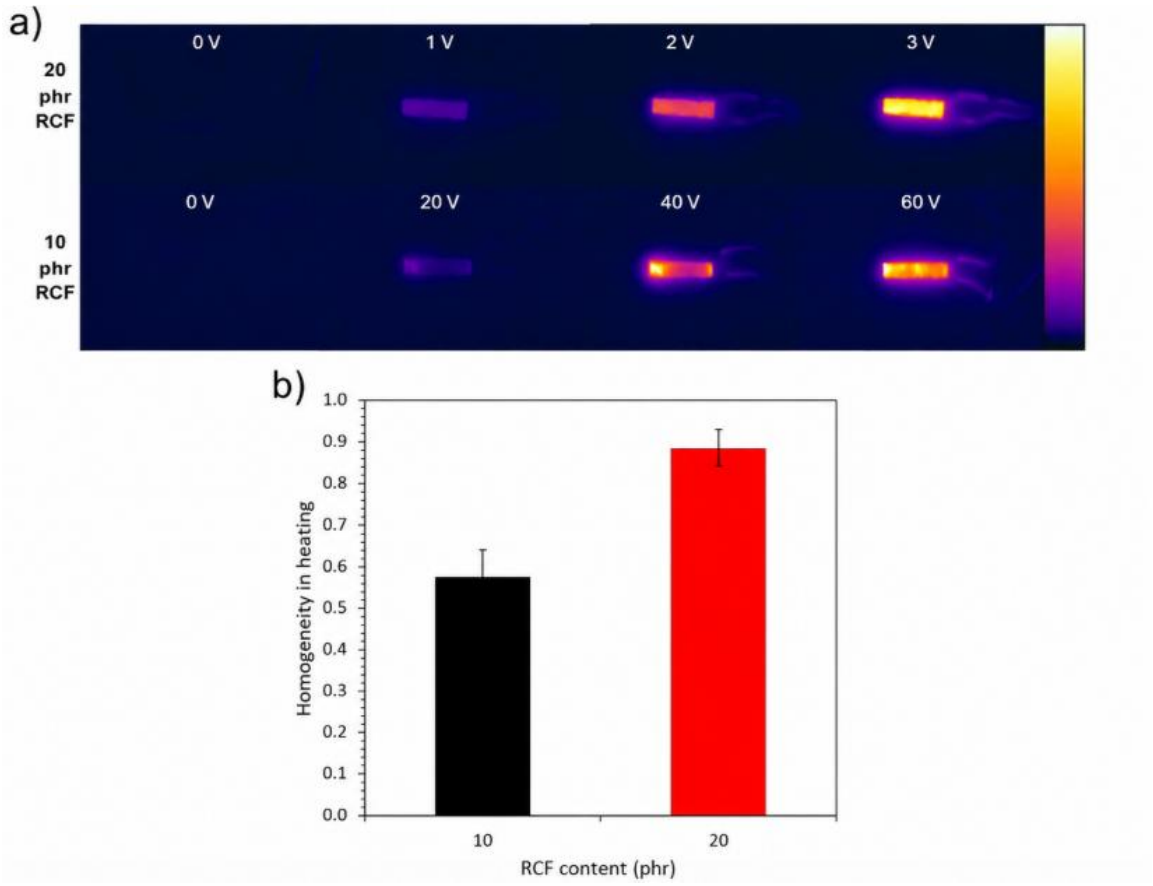

Figure 49 - joule heating homogeneity for DGEVA 10 and 20 phr of RCF content

Moving to the ECO matrix with regard to Joule heating, the measured values were consistent with the electrical conductivity observed at the corresponding points. For the 20 phr RCF formulation, it was not possible to detect any temperature increment even at 1000 V, which is directly related to the significantly lower electrical conductivity of 20 phr formulation, as previously explained in section 1.4. Consequently, Joule heating data were collected only for the 10 phr sample.

Figure 50 below shows the same trend observed for electrical conductivity as a function of increasing applied voltage. The main difference is that, in the ECO system, a slightly higher voltage was required to reach the same temperature levels observed in the DGEVA formulation.

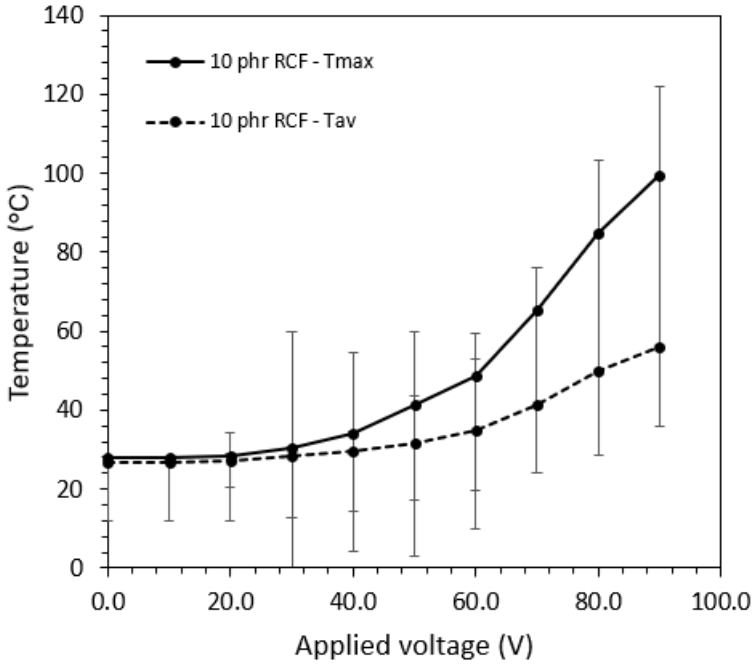

Figure 50 - Average and maximum temperatures reached by Joule heating in ECO

In this case, the heating behaviour of the composites was evaluated. Compared with the DGEVA system, the ECO formulation containing 10 phr of RCF exhibited a similar degree of temperature homogeneity and electrical conductivity when each system was operated at its maximum average achievable temperature. However, higher applied voltages were required for the ECO composite to reach comparable heating performances. As shown in the previous graphs, the maximum temperature achieved by the ECO system was approximately 100 °C, whereas the DGEVA-based composite reached temperatures close to 160 °C under comparable operating conditions. This difference can be attributed to the different electrical characteristics of the two polymer matrices, which influence the efficiency of Joule heating and ultimately limit the maximum attainable temperature of each system.

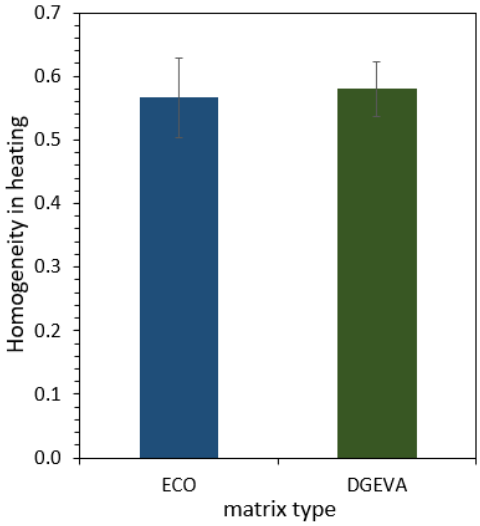

Figure 51 -Comparison of 10 phr RCF in the ECO and DGEVA matrices

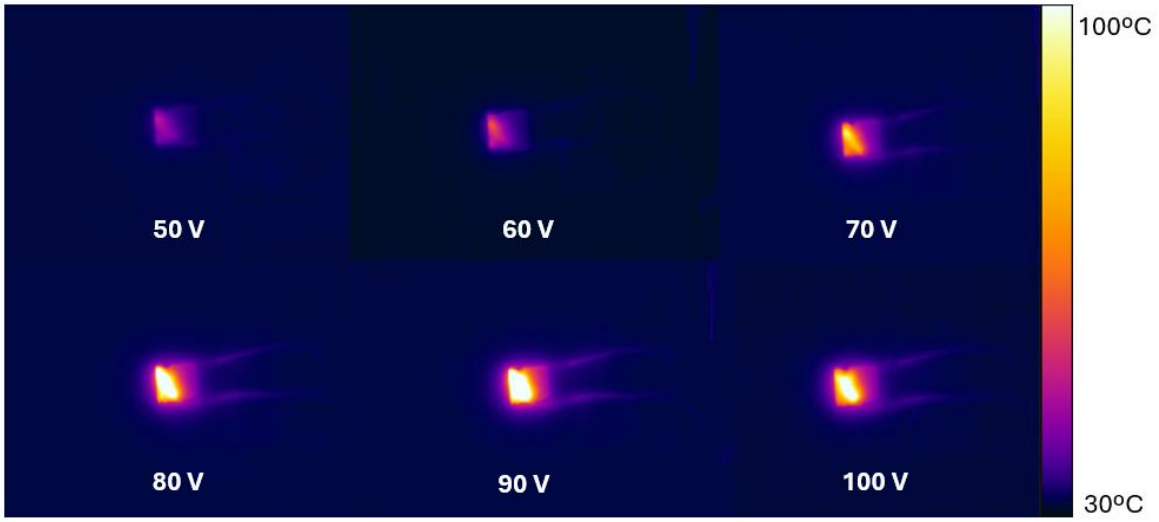

Figure 52 - Joule heating performance of the 10 phr RCF–ECO formulation

3.4 Covalent adaptable network evaluation

In this paragraph, the dynamic bonds of the two systems are analyzed. As described in the introductory section, for ECO and DGEVA the mechanisms of covalent adaptable networks are different: in the first case they are based on transesterification, while in the second they are due to disulfide bonds. These are therefore described separately in this section. The experiments were conducted within the linear viscoelastic region at temperatures ranging from 70 °C to 100 °C.

The dynamic nature of the bonds in ECO is governed by transesterification. Figure 53 shows, for all three systems (pristine, 10 and 20 phr), the shear relaxation modulus ($G(t)/G_0$) as a function of time. As expected, the relaxation rate for all systems decreases with increasing temperature. The characteristic relaxation time (τ) is defined as the time required for the modulus to decay to $1/e$ ($\approx 37\%$) of its initial value, as indicated by the dashed line. Moreover, for all formulations, a DBT-free reference system was specifically

prepared in order to highlight the different behaviour shown by the black curve in Figure 53.

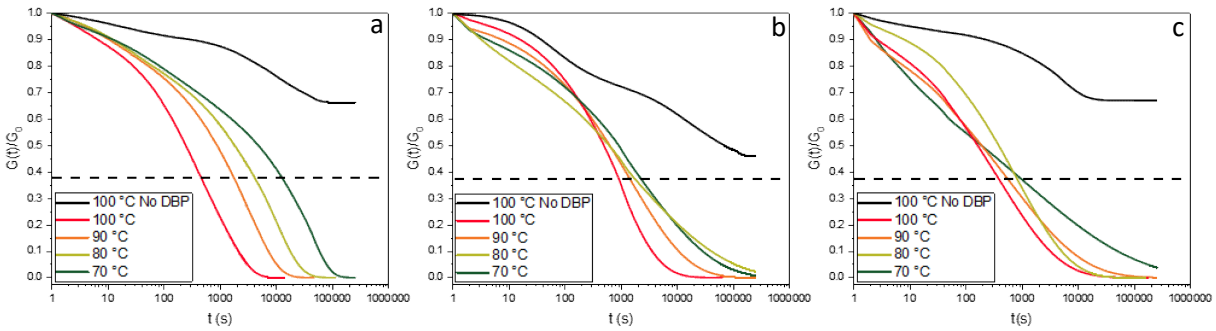

Figure 53 – ECO G(t)/G0 as a function of time for the pristine resin (a) and the composites reinforced with 10 (b) and 20 (c) phr of RCF

In this case, the material is never able to reach a decay below 1/e (≈37%) of its initial value within the investigated time window, clearly indicating that DBT is the key component enabling bond dynamics in the material.

The Arrhenius plot reported in Figure 54 exhibits a high degree of linear correlation ($R^2 \geq 0.97–0.99$), confirming the Arrhenius-type temperature dependence of the viscosity for all tested samples. The bond dynamics are therefore thermally activated, and the thermal response is governed by a well-defined energy barrier. The activation energy (Ea) is 112 kJ/mol for the formulation without filler, shows a decrease to 34 kJ/mol and 33 kJ/mol for the formulation with 10 and 20 phr RCF systems.

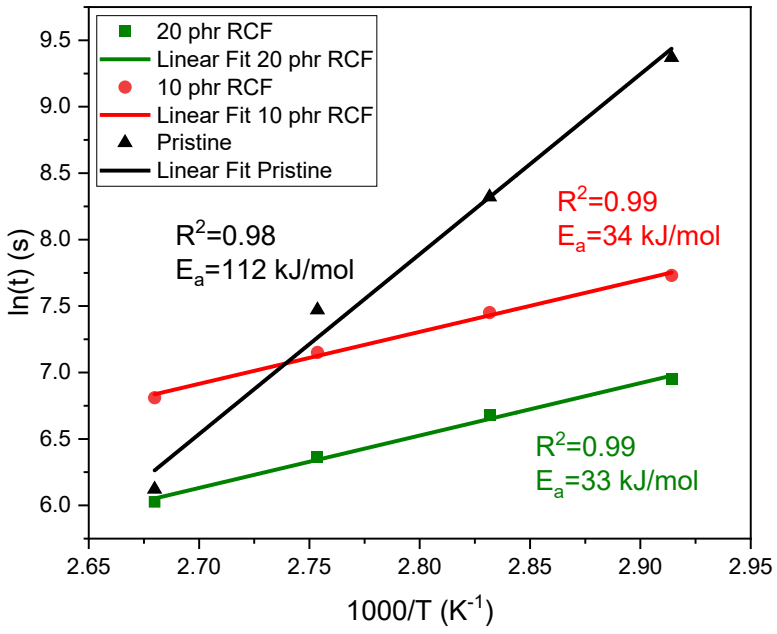

Figure 54 - Arrhenius plots for all the ECO samples

The dynamic nature of the DGEVA-4AFD network, imparted by the dynamic disulfide bonds (S–S) within the crosslinked structure, was also investigated through stress relaxation analysis. The experiments were conducted within the linear viscoelastic region at temperatures ranging from 130 °C to 160 °C.

Also in this case, Figure 55 (a–c) reports the normalized shear relaxation modulus ($G(t)/G_0$) as a function of time for the pristine resin and for the composites reinforced with 10 and 20 phr of RCF, respectively. As expected, the relaxation rate increased significantly with temperature. The characteristic relaxation time (τ) was determined as the time required for the modulus to decay to 1/e (≈37%) of its initial value (indicated by the dotted line).

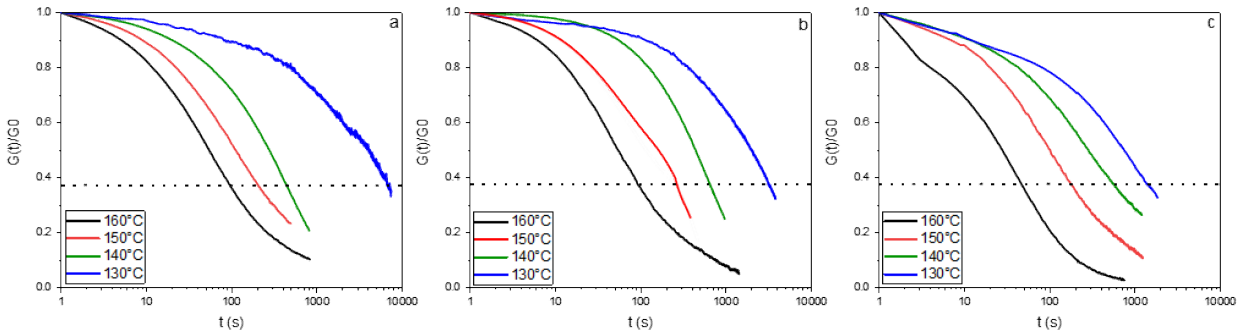

Figure 55 – DGEVA G(t)/G0 as a function of time for the pristine resin (a) and the composites reinforced with 10 (b) and 20 (c) phr of RCF

The Arrhenius plots reported in Figure 56 show good linearity ($R^2 \geq 0.97$), confirming that the viscosity of the samples follows an Arrhenius-type temperature dependence.

The neat matrix exhibits an activation energy (Ea) of 199 kJ/mol. The addition of RCF leads to a significant reduction in this value, which decreases to 165 kJ/mol for the 10 phr composite and to 163 kJ/mol for the 20 phr composite. This decrease indicates an easier relaxation process within the material.

This behavior can be explained by four main effects related to the presence of the filler.

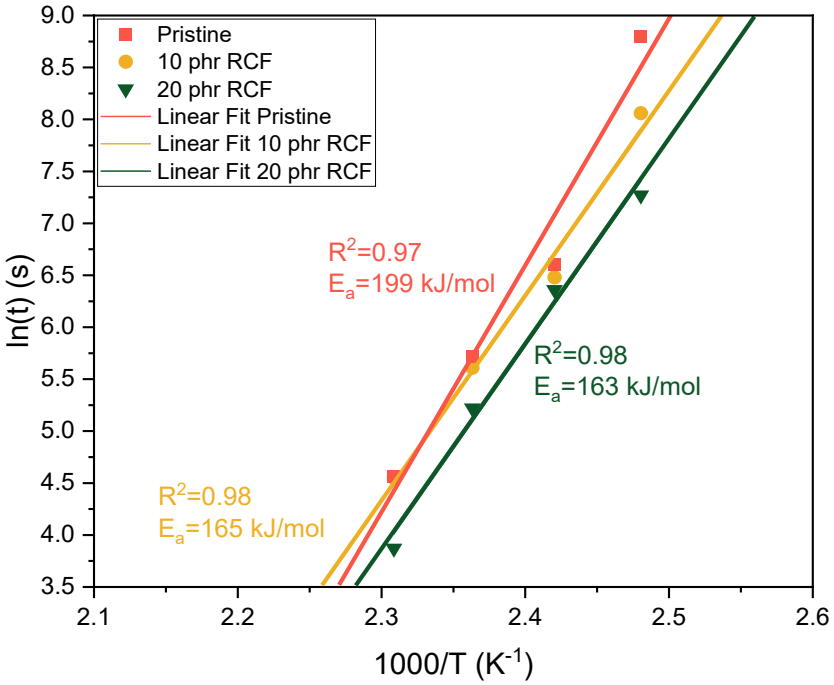

Figure 56 - Arrhenius plots for all the DGEVA samples

For both the ECO and DGEVA systems, the acceleration of stress relaxation observed with increasing RCF loading can be attributed to several concurrent factors.

First, recycled carbon fibers emerge from the recycling process with surfaces enriched in hydroxyl, carbonyl, and carboxyl functionalities, as well as traces of transition metal residues. These surface species can act as Brønsted or Lewis acid sites, promoting dynamic bond exchange reactions within the polymer network. This catalytic effect is particularly significant in the ECO system, where network rearrangement is governed by transesterification reactions. In contrast, the DGEVA system relies predominantly on disulfide exchange reactions, making the influence of these catalytic sites less pronounced.

Second, as the RCF content approaches the percolation threshold, the formation of a conductive graphitic network enhances heat transfer throughout the material. As a result, a more homogeneous temperature distribution is achieved during stress-relaxation experiments, leading to a faster network rearrangement and consequently to a lower apparent activation energy.

Third, the presence of fiber–matrix interfaces locally perturbs the epoxy network architecture, generating additional free volume and increasing chain mobility. This facilitates the bond-exchange processes responsible for stress relaxation.

Finally, the incorporation of RCF slightly affects the curing efficiency of the epoxy matrix, leading to a lower crosslinking density and a less constrained network structure. The increased mobility of the polymer chains further promotes dynamic bond rearrangement, contributing to the observed reduction in relaxation times and activation energy (51).

3.5 Self healing evaluation

As a complementary analysis, healing tests were first performed in a conventional oven and subsequently under Joule heating conditions, in order to enable localized repair of the coating and to evaluate its potential for final application scenarios.

Regarding the ECO system, some issues were encountered in obtaining a suitable geometry for profilometer analysis. Due to its low Tg, it was not possible to properly polish the surface to the required level of smoothness for accurate measurements. Therefore, as described in the Materials and Methods section, a non-conventional, macroscopic approach was adopted to evaluate the healing behaviour of the material.

Tensile tests were carried out using the setup shown in Figure 26 to assess the mechanical performance of the repaired specimens. Two processing conditions were investigated: 70°C for 30 min and 120°C for 6 h. The tensile load sustained by each specimen was measured, and the results are reported in Table 14 as the maximum load (N) supported by specimens of identical geometry.

RCF content (phr) in ECO matrix	tensile load [N]
Reference 10 phr RCF	0.51 ± 0.25
Reference 20 phr RCF	0.25 ± 0.10

RCF content (phr) in ECO matrix	First condition 70 °C - 30 min	Second condition 120 °C - 6 h
Partial overlap 10 phr RCF	0.4 ± 0.26	1.33 ± 0.7
Partial overlap 20 phr RCF	0.25 ± 0.04	1.04 ± 0.4

Table 14 - Tensile load measured for the reference specimens and for the partially overlapped ECO samples containing 10 and 20 phr of recycled carbon fibers (RCF) after healing treatments performed under different thermal conditions.

As shown in Figure 57 a), for the 10 phr sample under the first condition, the specimens used for the average calculation failed in the non-overlapping region, at slightly lower forces compared to the reference samples. This behaviour is likely due to a slightly reduced thickness in that section, suggesting that the healing process was successful.

Regarding the first condition at 20 phr, shown in Figure 57 c), a detachment of the upper part of the specimen can be observed. This is likely an indication that the fiber content and the selected time–temperature combination were not sufficient to achieve optimal healing.

Moving to the second condition Figure 57 (b-d), for both 10 phr and 20 phr, failure occurred near the joint, but at higher force levels. This is probably due to the fact that the effective cross-sectional area at the fracture location was approximately twice that of the reference specimen in both cases.

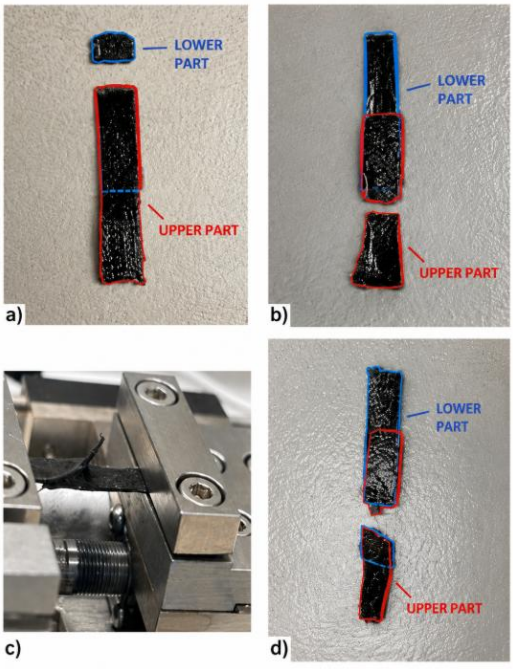

Figure 57 - Representative failure modes observed after tensile testing of partially overlapped ECO specimens: (a) cohesive failure within the lower part of the specimen ECO 10 phr RCF first condition – RCF, (b) cohesive failure at the overlap interface 20 phr first condition – RCF, (c) interfacial debonding (peeling) of the overlapping 10 phr second condition, (d) cohesive failure at the overlap interface 20 phr – RCF second condition

Moving to the DGEVA system, Figure 58 shows how the healing behaviour varies depending on whether the heating is carried out in an oven or via the Joule effect. It is also immediately evident that no healing data under Joule heating is reported for the formulation without conductive filler, since the polymer is electrically insulating and therefore cannot be heated via the Joule effect.

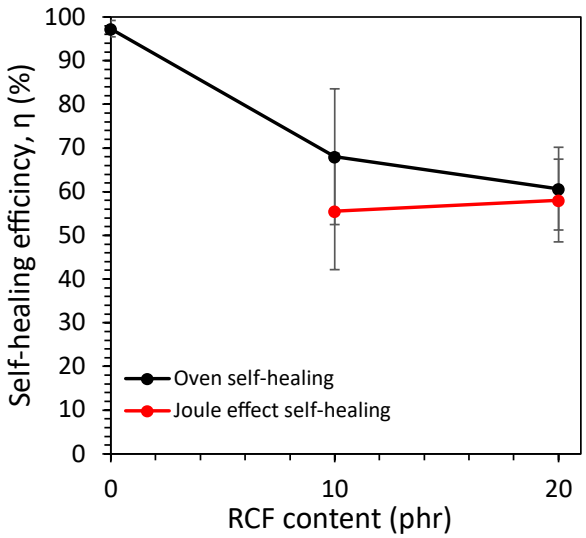

Figure 58 - Healing efficiency (η) as a function of recycled carbon fiber (RCF) content for specimens healed by conventional oven treatment and Joule-heating activation

Regarding the oven-heated tests, the pristine formulation exhibits healing values close to 100%, which progressively decrease with increasing carbon fiber content, reaching an average value of 60.7 %.

RCF content (phr) in DGEVA matrix	Oven self-heling [%]	Stdev
0	97.3	1.9
10	68.0	15.6
20	60.7	9.5

Table 15 - Oven-induced healing efficiency and corresponding standard deviations for DGEVA formulations with increasing RCF content.

This is likely due to the fact that the fibers hinder the dynamic exchange bonds present within the polymer matrix.

In contrast, when the tests were repeated using Joule heating, the opposite trend was observed, since as described in Section 3.3 the homogeneity of heat distribution increases with increasing carbon fiber content. In this way, heat is more uniformly delivered to reach the temperature required for the disulfide bond exchange responsible for the healing behaviour of the material.

RCF content (phr) in DGEVA matrix	Joule heating self-heling [%]	Stdev
0	0	0
10	55.5	13.3
20	58.0	9.5

Table 16 - Joule-heating healing efficiency and associated standard deviations for DGEVA formulations as a function of RCF content.

When comparing the different healing methods, Joule heating led to slightly lower η values than conventional oven heating, particularly for the samples reinforced with 10 phr RCF, due to the same heating homogeneity issues discussed above. Nevertheless, despite the slightly lower η achieved through Joule heating, this method provides a faster and more energy-efficient heating approach than conventional oven heating, while also enabling portable operation.

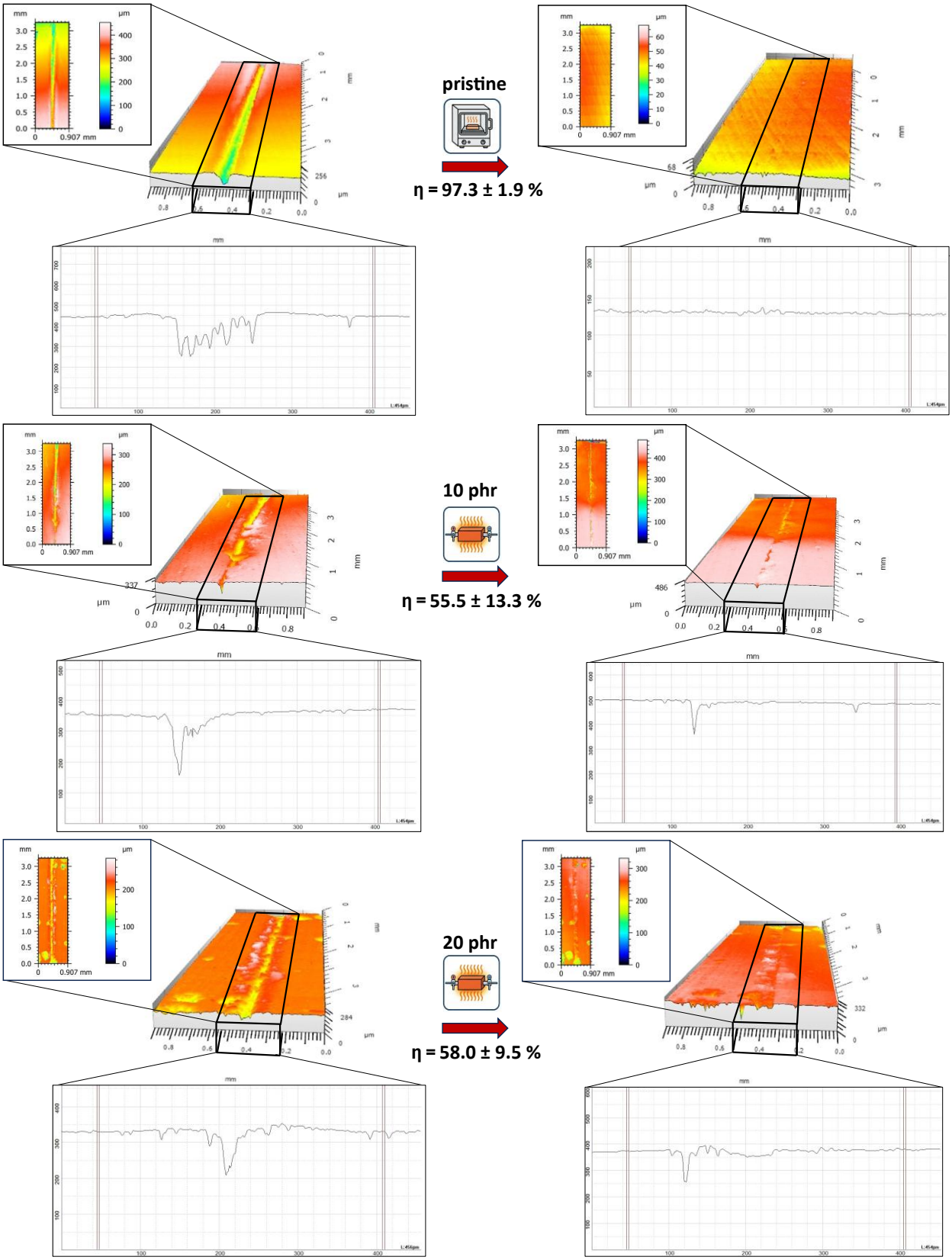

Figure 59 - Thermal maps and temperature profiles of pristine and RCF-reinforced DGEVA specimens before and after Joule-heating healing. The corresponding healing efficiencies are reported.

4. Conclusion

This work investigated two bio-based covalent adaptable network (CAN) systems reinforced with recycled carbon fibers (RCF): a UV-cured epoxidized castor oil (ECO) vitrimer based on transesterification reactions and a thermally cured diglycidyl ether of vanillyl alcohol (DGEVA) network based on disulfide exchange chemistry. The objective was to evaluate the influence of recycled carbon fibers on the thermal, mechanical, electrical, and healing properties of both matrices, with particular attention to the possibility of activating network rearrangement through Joule heating.

Despite the different curing mechanisms and dynamic chemistries involved, several common trends were observed. In both systems, the incorporation of RCF increased the stiffness of the material and provided electrical conductivity, enabling Joule-heating activation. Furthermore, both matrices retained their CAN character after fiber addition, demonstrating the possibility of combining sustainable bio-based polymers with recycled conductive reinforcements to obtain multifunctional materials.

Among the two investigated systems, DGEVA exhibited the most promising and consistent performance. The addition of recycled carbon fibers resulted in the expected increase in electrical conductivity, leading to more efficient and homogeneous Joule heating. Consequently, the conductive composites were able to reach the temperatures required for disulfide exchange reactions, promoting effective stress relaxation, network rearrangement, and healing. The healing efficiency obtained through Joule heating was comparable to, demonstrating the suitability of DGEVA-based composites for electrically triggered repair applications.

In contrast, the ECO-based composites displayed a less predictable behavior. Although CAN characteristics associated with transesterification reactions were preserved, the electrical response did not follow the expected trend with increasing fiber loading. Surprisingly, the formulation containing 10 phr of recycled carbon fibers exhibited higher conductivity than the 20 phr formulation. This behaviour also affected the Joule-heating performance, preventing a direct correlation between filler concentration and temperature increase.

A possible explanation can be found in the complex relationship between electrical conductivity and the characteristics of the polymer matrix. As discussed in the microstructural analysis, the electrical conductivity of polymer composites is not exclusively governed by filler concentration but is also strongly influenced by the morphology and integrity of the polymer matrix in the presence of the conductive filler. In the ECO system, the higher presence of internal voids and the lower degree of conversion observed in the formulation containing 20 phr of recycled carbon fibers, together with possible fiber agglomeration, may have hindered the formation of an efficient percolated conductive network. Consequently, increasing the fiber content did not necessarily result in improved electrical conductivity.

Overall, the results demonstrate that recycled carbon fibers can successfully transform bio-based CANs into electrically responsive materials capable of healing activation through Joule heating.

5. Reference

1. Alarcon RT, Cellai A, Porcarello M, Sölle B, Rossegger E, Schmitt CC, et al. Green Design of Renewable Dual-Curing Polymers with Healing and Recyclable Networks for 3D Printing. ACS Sustain Chem Eng. 2025 Sep 29;13(38):16136–53. doi:10.1021/ACSSUSCHEMENG.5C07154

2. Sangermano M, Bergoglio M, Schögl S. REVIEW www.mame-journal.de Biobased Vitrimeric Epoxy Networks [Internet]. 2023. doi:10.1002/mame.202300371

3. Cywar RM, Rorrer NA, Hoyt CB, Beckham GT, Chen EYX. Bio-based polymers with performance-advantaged properties. Nature Reviews Materials 2021 7:2. 2021 Sep 23;7(2):83–103. doi:10.1038/s41578-021-00363-3

4. Silva EAB da, Zabkova M, Araújo JD, Cateto CA, Barreiro MF, Belgacem MN, et al. An integrated process to produce vanillin and lignin-based polyurethanes from Kraft lignin. Chemical Engineering Research and Design. 2009 Sep 1;87(9):1276–92. doi:10.1016/J.CHERD.2009.05.008

5. Noè C, Hakkarainen M, Sangermano M. Cationic UV-Curing of Epoxidized Biobased Resins. Polymers 2021, Vol 13, Page 89. 2020 Dec 28;13(1):89. doi:10.3390/POLYM13010089

6. Law KL, Starr N, Siegler TR, Jambeck JR, Mallos NJ, Leonard GH. The United States' contribution of plastic waste to land and ocean. Sci Adv. 2020 Oct 28;6(44). doi:10.1126/SCIADV.ABD0288 PubMed PMID: 33127684.

7. Maeda T, Otsuka H, Takahara A. Dynamic covalent polymers: Reorganizable polymers with dynamic covalent bonds. Prog Polym Sci. 2009 Jul 1;34(7):581–604. doi:10.1016/J.PROGPOLYMSCI.2009.03.001

8. Ravve A. Light-associated reactions of synthetic polymers. Light-Associated Reactions of Synthetic Polymers. 2006;1–369. doi:10.1007/0-387-36414-5/SAVE-RESEARCH

9. uv-curing-technique.jpg (1600×900) [Internet]. [cited 2026 Jun 23]. Available from: https://www.iqsdirectory.com/articles/industrial-oven/curing-ovens/uv-curing-technique.jpg

10. Riccardo Cofano. Fotopolimerizzazione di coatings polimerici funzionali ottenuti da fonti bio-rinnov [Internet]. [cited 2026 Jun 23]. Available from: https://webthesis.biblio.polito.it/23085/1/tesi.pdf

11. Mendes-Felipe C, Oliveira J, Etxebarria I, Vilas-Vilela JL, Lanceros-Mendez S. State-of-the-Art and Future Challenges of UV Curable Polymer-Based Smart Materials for Printing Technologies. Adv Mater Technol. 2019 Mar 1;4(3):1800618. doi:10.1002/ADMT.201800618;WGROUP:STRING:PUBLICATION

12. Zhang Y hong, Zhai M jiao, Shi L, Lei Q yang, Zhang S tong, Zhang L, et al. Sustainable castor oil-based vitrimers: Towards new materials with reprocessability, healing, degradable and UV-blocking characteristics. Ind Crops Prod. 2023 Mar 1;193:116210. doi:10.1016/J.INDCROP.2022.116210

13. Chauhan J, Bhoi NK, Arora A, Singh MK, Siengchin S. Comprehensive review of curing methods in polymer composites: trends, challenges, and prospects. Polymer Bulletin 2026 83:7. 2026 May 7;83(7):397-. doi:10.1007/S00289-026-06464-9

14. Polymer Engineering - Google Libri [Internet]. [cited 2026 Jun 24]. Available from: https://books.google.it/books?hl=it&lr=&id=H6uYEAAAQBAJ&oi=fnd&pg=PA1&dq=Toward+the++recyclability+of+thermosetting+polymers.+In+Polymer+Engineering+&ots=j1NmpHwQkB&sig=hPq7mSNs7aMAPyHsNlP1gnX-vk8&redir_esc=y#v=onepage&q&f=false

15. Kamarulzaman S, Png ZM, Lim EQ, Lim IZS, Li Z, Goh SS. Covalent adaptable networks from renewable resources: Crosslinked polymers for a sustainable future. Chem. 2023 Oct 12;9(10):2771–816. doi:10.1016/j.chempr.2023.04.024

16. Montarnal D, Capelot M, Tournilhac F, Leibler L. Silica-like malleable materials from permanent organic networks. Science (1979). 2011 Nov 18;334(6058):965–8. doi:10.1126/SCIENCE.1212648;CSUBTYPE:STRING:SPECIAL;PAGE:STRING:ARTICLE/CHAPTER PubMed PMID: 22096195.

17. Alabiso W, Schlögl S. The Impact of Vitrimers on the Industry of the Future: Chemistry, Properties and Sustainable Forward-Looking Applications. Polymers 2020, Vol 12, Page 1660. 2020 Jul 26;12(8):1660. doi:10.3390/POLYM12081660

18. Imbernon L, Oikonomou EK, Norvez S, Leibler L. Chemically crosslinked yet reprocessable epoxidized natural rubber via thermo-activated disulfide rearrangements. Polym Chem. 2015;6:4271. doi:10.1039/c5py00459d

19. Tesoro GC, Sastri V. Reversible crosslinking in epoxy resins. I. Feasibility studies. J Appl Polym Sci. 1990 Apr 5;39(7):1425–37. doi:10.1002/APP.1990.070390702;SUBPAGE:STRING:ABSTRACT;WEBSITE:WEBSITE:PERICLES;WGROUP:STRING:PUBLICATION

20. Si H, Zhou L, Wu Y, Song L, Kang M, Zhao X, et al. Rapidly reprocessable, degradable epoxy vitrimer and recyclable carbon fiber reinforced thermoset composites relied on high contents of exchangeable aromatic disulfide crosslinks. Compos B Eng. 2020 Oct 15;199:108278. doi:10.1016/J.COMPOSITESB.2020.108278

21. Ruiz de Luzuriaga A, Solera G, Azcarate-Ascasua I, Boucher V, Grande HJ, Rekondo A. Chemical control of the aromatic disulfide exchange kinetics for tailor-made epoxy vitrimers. Polymer (Guildf). 2022 Jan 17;239:124457. doi:10.1016/J.POLYMER.2021.124457

22. Azcune I, Odriozola I. Aromatic disulfide crosslinks in polymer systems: Healing, reprocessability, recyclability and more. Eur Polym J. 2016 Nov 1;84:147–60. doi:10.1016/J.EURPOLYMJ.2016.09.023

23. Zhang Y, Yuan L, Liang G, Gu A. Developing Reversible Healing and Malleable Epoxy Resins with High Performance and Fast Recycling through Building Cross-Linked Network with New Disulfide-Containing Hardener. Ind Eng Chem Res. 2018 Sep 19;57(37):12397–406. doi:10.1021/ACS.IECR.8B02572

24. Ruiz De Luzuriaga A, Martin R, Markaide N, Rekondo A, Cabañero G, Rodríguez J, et al. Epoxy resin with exchangeable disulfide crosslinks to obtain reprocessable, repairable and

recyclable fiber-reinforced thermoset composites. Mater Horiz. 2016 May 3;3(3):241–7. doi:10.1039/C6MH00029K

25. Lu H, Wu Y, Qi X, Chi Z, Li Z, Xu L, et al. Thermally and light-triggered reconfigurable shape memory polydopamine/epoxy composite with healing and recyclable ability. J Appl Polym Sci. 2021 Jun 10;138(22):50526. doi:10.1002/APP.50526;REQUESTEDJOURNAL:JOURNAL:10974628;PAGE:STRING:ARTICLE/CHAPTER

26. Heaney MB. Resistance-expansion-temperature behavior of a disordered conductor–insulator composite. Appl Phys Lett. 1996 Oct 21;69(17):2602–4. doi:10.1063/1.117713

27. Scarisbrick RM. Electrically conducting mixtures. J Phys D: Appl Phys. 1973;6.

28. Xiao AY, Tong QK, Savoca AC, Van Oosten H. Conductive ink for through hole application. IEEE Transactions on Components and Packaging Technologies. 2001 Sep;24(3):445–9. doi:10.1109/6144.946492

29. Zhang W, Dehghani-Sanij AA, Blackburn RS. Carbon based conductive polymer composites. Journal of Materials Science 2007 42:10. 2007 Mar 31;42(10):3408–18. doi:10.1007/S10853-007-1688-5

30. Sau KP, Chaki TK, Khastgir D. Carbon fibre filled conductive composites based on nitrile rubber (NBR), ethylene propylene diene rubber (EPDM) and their blend. Polymer (Guildf). 1998 Dec 1;39(25):6461–71. doi:10.1016/S0032-3861(97)10188-4

31. Sau KP, Chaki TK, Khastgir D. Conductive rubber composites from different blends of ethylene-propylene-diene rubber and nitrile rubber. Journal of Materials Science 1997 32:21. 1997 Nov 1;32(21):5717–24. doi:10.1023/A:1018613600169

32. Narkis M, Vaxman A. Resistivity behavior of filled electrically conductive crosslinked polyethylene. J Appl Polym Sci. 1984 May 1;29(5):1639–52. doi:10.1002/APP.1984.070290518;WGROUP:STRING:PUBLICATION

33. Pourhashem S, Saba F, Duan J, Rashidi A, Guan F, Nezhad EG, et al. Polymer/Inorganic nanocomposite coatings with superior corrosion protection performance: A review. Journal of Industrial and Engineering Chemistry. 2020 Aug 25;88:29–57. doi:10.1016/J.JIEC.2020.04.029

34. Hwang JJ, Wu CY, Hung YH, Li MX, Luo KH, Jia HW, et al. Biomimetic PMMA coating surface and its application on inhibition of bacterial attachment and anti-biofilm performance. Surfaces and Interfaces. 2023 Feb 1;36:102548. doi:10.1016/J.SURFIN.2022.102548

35. Asadi H, Suganthan B, Ghalei S, Handa H, Ramasamy RP. A multifunctional polymeric coating incorporating lawsone with corrosion resistance and antibacterial activity for biomedical Mg alloys. Prog Org Coat. 2021 Apr 1;153:106157. doi:10.1016/J.PORGCOAT.2021.106157

36. Lan C, Zou L, Wang N, Qiu Y, Ma Y. Multi-reflection-enhanced electromagnetic interference shielding performance of conductive nanocomposite coatings on fabrics. J Colloid Interface Sci. 2021 May 15;590:467–75. doi:10.1016/J.JCIS.2021.01.074 PubMed PMID: 33561596.

37. Zhang Z, Li Z, Zhang M, Hao H, Yan S. Resistance-type strain sensor based on carbon nanofiber/polypyrrole composite membrane with high sensitivity. Polym Compos. 2024 Jul 10;45(10):8876–88. doi:10.1002/PC.28382

38. Wang F, Yang B, Zhang Z, He Q, Zhang Y. Synergistic effect of hybrid fillers on electro-thermal behavior of nanocomposite for active de-icing application. Composites Communications. 2021 Jun 1;25. doi:10.1016/J.COCO.2021.100746

39. Parent O, Ilinca A. Anti-icing and de-icing techniques for wind turbines: Critical review. Cold Reg Sci Technol. 2011 Jan 1;65(1):88–96. doi:10.1016/J.COLDREGIONS.2010.01.005

40. Martinez-Diaz D, Espeute E, Jiménez-Suárez A, Prolongo SG. Electrical and Joule Heating Capabilities of Multifunctional Coatings based on Recycled Carbon Fiber from Prepreg Scrap. ACS Omega. 2023 Dec 12;8(49):46548–59. doi:10.1021/ACSOMEGA.3C05413

41. Genua A, Montes S, Azcune I, Rekondo A, Malburet S, Daydé-Cazals B, et al. Build-To-Specification Vanillin and Phloroglucinol Derived Biobased Epoxy-Amine Vitrimers. Polymers 2020, Vol 12, Page 2645. 2020 Nov 10;12(11):2645. doi:10.3390/POLYM12112645

42. Guggari S, Magliozzi F, Malburet S, Graillot A, Destarac M, Guerre M. Vanillin-Based Epoxy Vitrimers: Looking at the Cystamine Hardener from a Different Perspective. ACS Sustain Chem Eng. 2023 Apr 17;11(15):6021–31. doi:10.1021/ACSSUSCHEMENG.3C00379

43. Gabbott P. Principles and Applications of Thermal Analysis. Principles and Applications of Thermal Analysis. 2008 Apr 16;1–388. doi:10.1002/9780470697702

44. Bergoglio M, Reisinger D, Schlögl S, Griesser T, Sangermano M. Sustainable Bio-Based UV-Cured Epoxy Vitrimer from Castor Oil. Polymers 2023, Vol 15, Page 1024. 2023 Feb 18;15(4):1024. doi:10.3390/POLYM15041024

45. Porcarello M, Greco E, Cellai A, Turra Alarcon R, Rossegger E, Sangermano M. 3D printing with biobased epoxidized formulations based on vegetable oils with dynamic polymer network properties. Polym Chem. 2026 Mar 3;17(9):911–22. doi:10.1039/D5PY01069A

46. Handbook of Thermal Analysis and Calorimetry: Applications to Polymers and ... - Google Libri [Internet]. [cited 2026 Jun 25]. Available from: https://books.google.it/books?hl=it&lr=&id=Xiypn61kFpMC&oi=fnd&pg=PP1&dq=Thermal+Analysis+of+Polymers:+Fundamentals+and++Applications,+Hoboken+New+Jersey,&ots=oXQNNcA_cv&sig=9Sqt5WThfPvuIfYifXRIe2lRAjo&redir_esc=y#v=onepage&q&f=false

47. Pezzana L, Melilli G, Delliere P, Moraru D, Guigo N, Sbirrazzuoli N, et al. Thiol-ene biobased networks: Furan allyl derivatives for green coating applications. Prog Org Coat. 2022 Dec 1;173:107203. doi:10.1016/J.PORGCOAT.2022.107203

48. Thermal Analysis Tools. Thermal Analysis of Polymeric Materials. 2005 Nov 11;279–454. doi:10.1007/3-540-26360-8_4

49. Liu X, Yang X, Wang S, Wang S, Wang Z, Liu S, et al. Fully Bio-Based Polyhydroxyurethanes with a Dynamic Network from a Terpene Derivative and Cyclic

Carbonate Functional Soybean Oil. ACS Sustain Chem Eng. 2021 Mar 22;9(11):4175–84. doi:10.1021/ACSSUSCHEMENG.1C00033

50. Theophanides T. INFRARED SPECTROSCOPY – MATERIALS SCIENCE , ENGINEERING AND Edited by Theophile Theophanides. 2012;524.

51. Cellai A, Alarcon RT, Sölle B, Rossegger E, Casalegno V, Salvo M, et al. Biobased Epoxidized Castor Oil Covalent Adaptable Networks Adhesives Reinforced with Recycled Carbon Fibers. Macromol Rapid Commun. 2025;e00790. doi:10.1002/MARC.202500790;SUBPAGE:STRING:FULL

6. Acknowledgements

I would like to express my sincere gratitude to Professor Marco Sangermano for giving me the opportunity to carry out this research project and for his continuous support and guidance throughout this work.

My special thanks go to Alberto for welcoming me into the research group from the beginning and for his constant support, patience, and valuable advice throughout the project.

I would also like to thank Professor Alberto Jiménez Suárez, Alejandro Cortez, and all the colleagues at Universidad Rey Juan Carlos for welcoming me to Madrid, sharing their knowledge, and making this research experience both professionally and personally enriching.

I am deeply grateful to my parents and my brother for teaching me the value of commitment and perseverance and for always encouraging me to follow my own path.

I would also like to thank my university classmates for their support and friendship throughout these years.

A heartfelt thank you goes to my lifelong friends Giorgia, Martina, and Chicca, to Vittoria for her constant advice and support.

Finally, I would like to thank Riccardo for being by my side throughout this journey, encouraging me to embrace new challenges and supporting me during every stage of this experience.

Last but not least, I would like to thank everyone who, in different ways, has contributed to my personal and professional growth over the years.